ANELASTIC STUDIES OF INTERSTITIALLY TRAPPED HYDROGEN IN NIOBIUM

BY

PHILIP EMERSON ZAPP

A.B., Cornell University, 1971

THESIS

Submitted in partial fulfillment of the requirements
for the degree of Doctor of Philosophy in Metallurgical Engineering
in the Graduate College of the
University of Illinois at Urbana-Champaign, 1979

Urbana, Illinois

DISCLAIMER

UNIVERSITY OF ILLINOIS AT URBANA-CHAMPAIGN

THE GRADUATE COLLEGE

MARCH, 1979

WE HEREBY RECOMMEND THAT THE THESIS BY

PHILIP EMERSON ZAPP

ENTITLED ANELASTIC STUDIES OF INTERSTITIALLY TRAPPED HYDROGEN IN NIOBIUM

BE ACCEPTED IN PARTIAL FULFILLMENT OF THE REQUIREMENTS FOR THE DEGREE OF DOCTOR OF PHILOSOPHY

H K Birnbaum
Director of Thesis Research

C G West
Head of Department

Committee on Final Examination†

H K Birnbaum
Chairman

C. G. West

E N Pugh

A. V. Granato

†Required for doctor's degree but not for master's.

O-317

ACKNOWLEDGEMENTS

The author gratefully acknowledges the guidance and support of his thesis adviser, Professor Howard K. Birnbaum. Helpful discussions with many present and former colleagues in the Department of Metallurgy and Mining Engineering are also acknowledged.

The author wishes to express his gratitude to his parents for their support, and he thanks his wife, Marlene, for her indispensable, loving encouragement.

This project was supported by the U.S. Department of Energy, contract DOE-EY-76-C-02-1198, through the Materials Research Laboratory, University of Illinois at Urbana-Champaign.

TABLE OF CONTENTS

1. INTRODUCTION

Research into the diffusion of hydrogen in metals has intensified over the last decade for both technological and intellectual reasons. Knowledge of the diffusive behavior of hydrogen is important to the explanation of the hydrogen embrittlement of metals, to the resolution of materials problems which will be encountered in the production of energy from the chemical and nuclear burning of hydrogen, and to the use of metal hydrides as energy storage media. Among the facts and observations that motivate basic scientific interest is the large value of the diffusion coefficient itself.[1] At room temperature the diffusion coefficient of hydrogen in niobium exceeds those of oxygen and nitrogen in niobium by more than fifteen orders of magnitude. Furthermore there is strong evidence for a quantum mechanical motion of hydrogen in niobium below 60K.[2] Hydrogen atoms have also been shown to be strongly trapped by other point defects and by dislocations,[3] and this trapping affects the diffusivity.

The subjects of trapping and quantum mechanical motion of hydrogen are investigated in the present work in the systems Nb-O-H and Nb-N-H, by the technique of anelastic relaxation. In all experiments the measured relaxations were caused by the local, stress-induced reorientation of single hydrogen atoms bound to single, essentially immobile oxygen and nitrogen atoms.[4] The symmetries and binding enthalpies of O-H pairs

were studied in oriented single crystals of high-purity niobium; the technique used was the pulse-echo attenuation of very-high frequency longitudinal stress waves between 100 and 300K. Well-defined internal friction peaks were found in the ⟨100⟩, ⟨110⟩, and ⟨111⟩ directions of the b.c.c. lattice. The temperature dependence of the jump frequency of hydrogen below 100K was studied in the Nb-N-H system using lower frequency methods. Internal friction peaks were measured in the frequency range 3 to 165 Hz, and relaxation times were calculated from strain relaxation measurements at temperatures below 60K. These data show marked deviations from classical thermally activated Arrhenius behavior.

2. REVIEW OF PREVIOUS EXPERIMENTS

2.1 Methods

Among the methods discussed in reference (1) for the investigation of hydrogen diffusion in b.c.c. metals, perhaps the most productive, near and below room temperature, have been those that measure anelastic relaxations. While the mobility of hydrogen is certainly high enough for the use of bulk methods, surface oxides and nitrides are inescapable at these temperatures.[5] It is very likely that the oxides and nitrides are partly responsible for the high and inconsistent values of the activation enthalpy for hydrogen motion determined with these methods.[6] The anelastic methods do not involve transfer across surfaces. They can be applied in the study of diffusion through an exceptionally wide range of reciprocal temperatures and to a range of phenomena from long-range diffusion to local reorientation around point and line defects.

Two categories of anelastic relaxation may be attributed to the motion of hydrogen in metals according to whether the motion occurs over macroscopic or microscopic distances. Long-range diffusion may occur in response to a nonuniform applied stress (in general of both shear and normal character) as the defects migrate to lower the free energy of the system. The migration forms a concentration gradient which dissipates upon removal of the external stress, causing the relaxation. This phenomenon is known as the Gorsky effect,[7] a recent review

which has been written by Völkl.[8] Since the diffusion occurs over macroscopic distances, reasonable relaxation times obtain only for species with high mobility, such as hydrogen and its isotopes. If the strain field of a defect has a lower point group symmetry than the host lattice, and if there exists more than one site for the defect, anelastic relaxation will occur when an appropriate stress induces diffusion, or ordering, of the defect into the energetically preferred site. Many types of point and line defects cause relaxations in this manner; the stress-induced reorientation of atoms of carbon, nitrogen, and oxygen in the b.c.c. metals is the well-known Snoek effect.[9]

Both elastic after-effect (or strain relaxation) and internal friction techniques have been applied to the measurement of the Gorsky effect and local reorientations due to hydrogen in niobium. In the Gorsky effect the diffusion coefficient, D, is directly related to the measured relaxation time, τ, by the equation $\tau = \alpha \ell^2/D$, where α is a constant, and ℓ is the characteristic dimension over which diffusion occurs. However, in studies of local reorientation, the relation between relaxation time and diffusivity is not so simple, for the jump distance must be known, and it must be ascertained that the local reorientation process is a part of the long-range migration. Results of the anelastic methods will be discussed in the succeeding sections.

Solid solution hydrogen increases the resistivity of niobium by 0.75 $\mu\Omega$-cm/at.%.[10] This property can be used in the study

of diffusion by measuring the time-rate of change of a specimen's resistance and in solubility and trapping studies, results of which will also be discussed. Finally useful information on diffusion and trapping of hydrogen in niobium can be obtained from measurements of the broadening of the energy distribution of quasi-elastically scattered neutrons.[11]

2.2 Local Reorientation of Hydrogen

Internal friction studies of the local reorientation of carbon, oxygen, and nitrogen in b.c.c. metals have been quite successful.[12] In addition to measurements of the Snoek effect,[13] reorientation of small clusters of oxygen atoms has been observed in tantalum[14] and in niobium.[15] As interest in the behavior of hydrogen has increased, several attempts have been undertaken to measure a Snoek effect due to that element in the Group Va metals, under the assumption that occupation of the same interstices in b.c.c. metals as O and N would give rise to such a relaxation peak.

Early work on the internal friction of hydrogen in niobium revealed a peak near 100K in the kilohertz frequency range that was interpreted as a Snoek peak.[16-18] The purity of the alloys used in these studies may be generally considered low with significant amounts of impurities such as oxygen and nitrogen probably present. The activation enthalpy for motion of 0.18 eV/atom calculated by Cannelli and Verdini[16] is much larger than that derived from Gorsky effect measurements

(0.068 eV/atom for T < 250K) which reflected the motion of single hydrogen atoms.[19]

More recent experiments on local reorientation have established the trapped hydrogen atom as the species causing relaxation.[3,4,20] Baker and Birnbaum[3] used a megahertz-range pulse-echo internal friction technique and a kilohertz-range flexural method to measure damping peaks in niobium specimens with various H, O, and N concentrations. The peaks were attributed to H-H pairs and to O-H or N-H pairs by analysis of the concentration dependence of the peak heights. Motion of the H-H pairs from 100 to 200K was characterized by an activation enthalpy of 0.055 eV/atom; for O(N)-H pairs the activation enthalpy was 0.165 eV/atom between 150 and 200K. Deviations from a classical Arrhenius temperature dependence toward enhanced jump frequencies were observed in the data for the O(N)-H pair (below 100K) and for the H-H pair (below 50K). This was interpreted as evidence for quantum mechanical tunnelling, but the presence of hydrides and uncertainties about the compositions made the interpretation somewhat speculative.

The pulse-echo method was used by Mattas and Birnbaum[4] to study the motion of H atoms in well-characterized, ⟨100⟩ oriented single crystals of niobium doped with oxygen. Linear dependences both in the oxygen (for $C_O < C_H$) as well as hydrogen concentrations (with $C_O > C_H$) for the heights of the damping peaks confirmed that the relaxation arose from the reorientation of single hydrogen atoms about single, immobile oxygen atoms, with

an activation enthalpy of 0.16 eV/atom. A binding enthalpy for the O-H pair was calculated to be 0.09 eV/atom, under the assumption of a small concentration of paired hydrogen relative to unpaired hydrogen. Internal friction peaks due to deuterium-oxygen pairs were also measured. The data revealed a marked nonclassical isotope effect. Large isotopic mass dependences were seen in both the preexponential factor and the activation enthalpy of the Arrhenius relations for H and D motion. The activation enthalpy for O-D reorientation was 25% larger than that for O-H reorientation.

A later investigation by Schiller and Schneiders[20] has corroborated the reorientation of O-H clusters as the mechanism causing relaxation near 100K at frequencies in the kilohertz range. Their data showed that for an O concentration of 0.06 at.% the relaxation strength increases to a maximum with increasing hydrogen content after which it levels off to 40% of the maximum for $C_H > 1$ at.%. The maximum having occurred at about 0.2 at.% H, it was concluded that more than one hydrogen atom may reorient about a single oxygen atom. Work by Schiller and Nijman[21] briefly examined the orientation dependence of the O-H internal friction peak in order to determine the structure of the defect. The concentrations appear to have been (from estimate of the height of the oxygen Snoek peak) about 0.02 at.% O and 0.1 at.% H. Measurements on a flexure specimen with stress axis parallel to the ⟨100⟩ direction showed the oxygen Snoek peak and a faintly detectable low temperature

peak ($Q^{-1} < 3 \times 10^{-5}$), while measurements on a specimen with a ⟨111⟩ orientation revealed a peak at 80K and 1270 Hz ($Q^{-1} \simeq 2.7 \times 10^{-4}$) but no Snoek peak. Also a hydride precipitation peak was identified in each specimen. The data suggest that alignment of the O-H pair along a ⟨111⟩ direction (i.e., trigonal point symmetry) is the stable configuration of this defect. However, the small peak height estimated for the ⟨100⟩ specimen is in fact in good agreement with the measured relaxation strength of Mattas and Birnbaum,[4] if account is taken of the low oxygen concentration in the samples of Schiller and Nijman. An activation enthalpy of motion could not be estimated from the latter authors' data.

Internal friction and strain relaxation techniques were used by Chen and Birnbaum to study the local jumping at low temperatures of oxygen-trapped hydrogen in niobium.[22] Between 60 and 80K the hydrogen jump frequency (ranging from 3 to 150 Hz) agreed with the Arrhenius behavior established by the megahertz and kilohertz frequency data (Figure 1). At temperatures below 50K, however, a marked deviation towards higher jump frequencies obtained. The data have been analyzed in terms of the phonon-assisted tunnelling theory of Flynn and Stoneham.[22] A least-squares fit of data from references (2, 4, 16, and 17) to the theory yields three parameters: the lattice activation enthalpy E_a = 0.211 eV/atom, the Debye temperature θ_D = 263.6K, and the transition matrix element $|J|$ = 0.0535 eV. E_a is related to, but not equivalent to, the classical activation enthalpy of the

Figure 1. The logarithm of the hydrogen jump frequency around oxygen versus reciprocal temperature. O, Ref. (4); Δ, Ref. (16); □, Ref. (17); ●, Ref. (2). After Chen and Birnbaum (2).

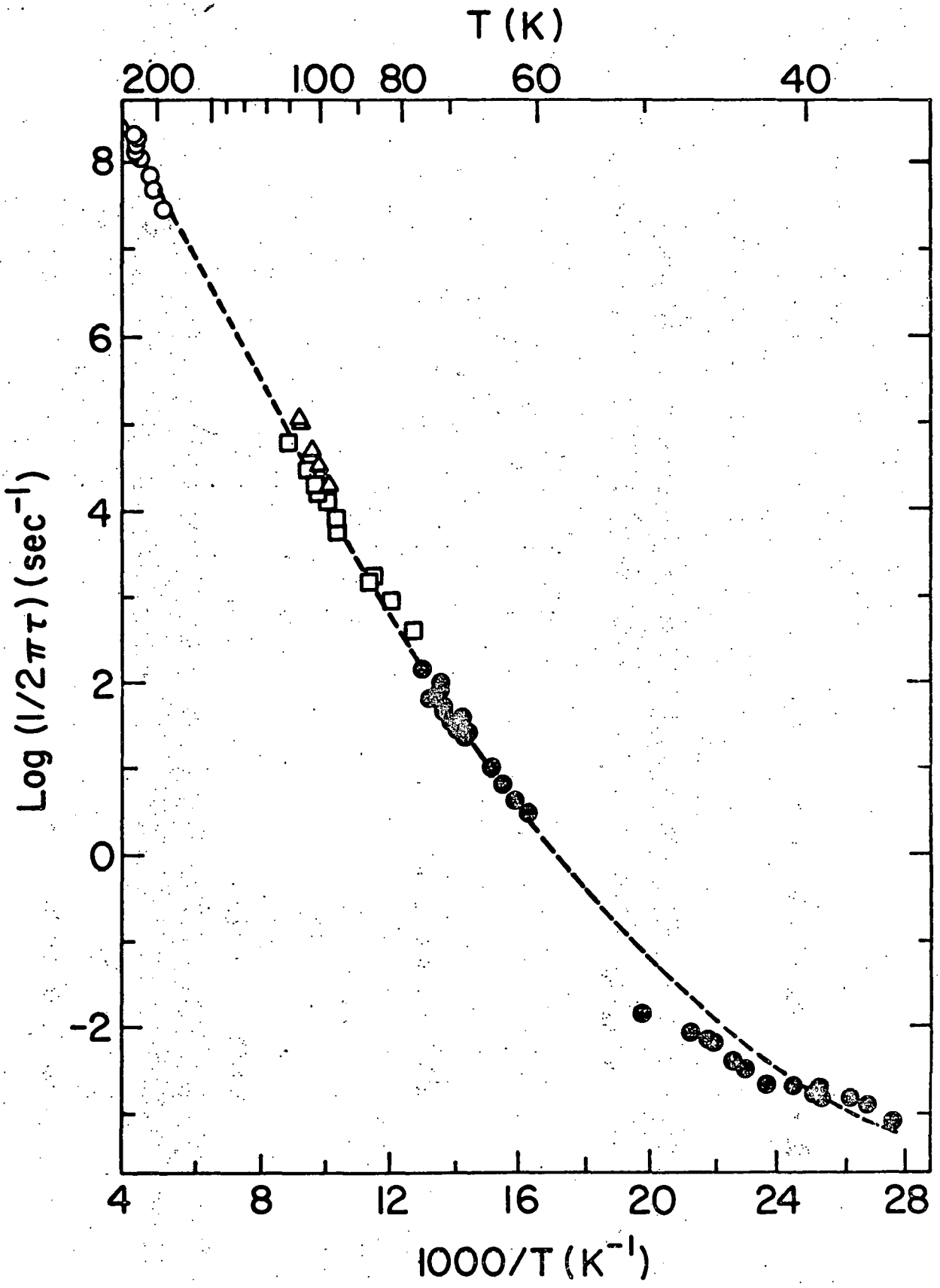
T (K)
200
100
80
60
40
8
6
4
2
0
-2
Log (1/2πτ) (sec⁻¹)
4
8
12
16
20
24
28
1000/T (K⁻¹)

high temperature data plotted as an Arrhenius function. It actually measures the self-trapping energy of the hydrogen interstitial. The value of θ_D is about 4% less than that determined from heat capacity measurements on pure niobium,[23] and the value of $|J|$ was concluded to be theoretically reasonable.[22]

Quantum effects have been deduced from the data on the diffusion of hydrogen in iron[24] and in tantalum.[25] Recently the technique of magnetic relaxation has been applied in a study of the motion of hydrogen clusters and of carbon-trapped hydrogen in iron.[26] The temperature dependence of the hydrogen jump frequency around the C interstitial was found to be unreasonably small in a classical Arrhenius analysis, while the power law dependence of jump frequency upon temperature[22] expected from the phonon-assisted tunnelling gave a good fit to the data. Further evidence of quantum behavior of hydrogen in niobium may be seen in recent experiments on megahertz-range internal friction at temperatures below 10K.[27] Damping peaks have been found in single crystals of Nb doped with H and O which can be ascribed to transitions of a delocalized hydrogen atom among energy levels associated with a ring of tetragonal and triangular interstices.[28] Additional support for this tunneling model is provided by heat capacity measurements.[29,30]

Thus far a hydrogen Snoek peak has not been convincingly demonstrated. The very high jump frequencies of H in niobium suggest that a Snoek effect, if it exists, would occur at such

low temperatures that only a few appm of hydrogen would remain in solid solution,[31] resulting in a proportionally small relaxation. However, at temperatures where several atomic percent hydrogen may exist in the α-phase, evidence for a Snoek relaxation can be sought in measurements of the elastic constants as functions of temperature.[32] Buchholz et al. have measured the shear modulus G of pure Ta and H-doped Ta.[33] From their results an upper bound for the normalized anisotropy of the H strain field was calculated to be 0.08 compared to about 0.9 for O and N in Nb. Measurements of diffuse x-ray scattering give an upper bound for the normalized anisotropy of 0.057.[34] A nearly cubic strain field is also implied by results of quasi-elastic neutron scattering.[35]

A tetragonally symmetric strain field for hydrogen in the b.c.c. metals is expected because of the tetragonal symmetry of both the tetrahedral and octahedral interstices that can be occupied by hydrogen. The seeming absence of the tetragonality may result from the rapid jump rates of hydrogen which do not allow sufficient time to develop an anisotropic strain field around any one site.[33] It has been suggested also that the hydrogen atom is not really localized on a particular site but is spread over a ring of tetrahedral and triangular sites centered upon an octahedral position.[28] Such a ring has been shown to possess a fairly cubic strain field.

2.3 Gorsky Effect and Resistivity Experiments

Long-range diffusion of hydrogen in niobium has been measured between 120K and 800K by means of the Gorsky effect. Cantelli et al.[36] found an Arrhenius temperature dependence of the diffusion coefficient between 250K and 800K with an activation enthalpy of 0.109 eV/atom, a value which is in excellent agreement with that of Schaumann et al.[19] The latter, however, found that the activation enthalpy decreases rather abruptly at 250K to 0.068 eV/atom, which characterizes their data down to 120K. Matusiewicz et al.[37] in measurements over a smaller temperature range than Schaumann et al. did not observe this change, though the agreement among the values of the diffusion coefficients is very good. Recent low temperature measurements in the Ta-H and Ta-D systems also reveal a decrease to a low activation enthalpy.[38] In the Nb-H system (the change has not been seen in the Nb-D system) measurements of resistivity relaxation by Wipf and Alefeld[39] have verified the activation enthalpy values of Schaumann et al.

No satisfactory explanation of this change in activation enthalpy exists. Münzing et al.[40] have shown that additions of nitrogen raised the low temperature enthalpy ultimately to the high temperature value, perhaps by a trapping interaction. However it was noted that the amount of nitrogen, not the nitrogen-hydrogen ratio was the significant parameter in depressing the low temperature diffusion. The activation enthalpy of motion was shown to depend linearly upon the concentration

of oxygen traps,[37] and neutron scattering experiments have shown that nitrogen doping lowers the low temperature diffusivity of hydrogen in niobium.[41] These results were explained by the trapping of H at N with a binding enthalpy of 0.1 eV.

The binding of hydrogen to nitrogen trap sites in niobium has been studied by Pfeiffer and Wipf using resistivity measurements.[42] It was found that when $C_N > C_H$ precipitation of niobium hydride was inhibited by the retention of hydrogen in solid solution at the nitrogen traps. A model of trapping was discussed in which only one H atom may be bound to a N atom; the binding enthalpy was calculated to be 0.12 eV/atom. Measurements of the resistivity recovery of quenched hydrogen in niobium by Hanada[43] have confirmed the suppression of precipitation when $C_N > C_H$, but it was concluded from the amount of recovery as a function of the H concentration that up to four H atoms may be bound to a N atom. Major recovery stages were found to occur in the Nb-O-H and Nb-N-H systems at 70K and 90K respectively; it appears, therefore, that nitrogen is a deeper trap for hydrogen than is oxygen.

3. THEORY

3.1 The Standard Anelastic Solid

Anelasticity adds to ideal elasticity a time dependence between stress and strain, while retaining the properties of complete recoverability of response and linearity of the stress-strain relationship. Thus, in the simplest case of time dependence, Hooke's law for ideal elastic behavior is modified by the addition of first time derivatives of stress and strain

$$\varepsilon + \tau_\sigma \dot{\varepsilon} = J_R \sigma + \tau_\sigma J_U \dot{\sigma} \qquad (1)$$

where the constants τ_σ, J_R, and J_U are the relaxation time at constant stress, the relaxed elastic compliance, and the unrelaxed elastic compliance, respectively. Equation (1) defines the response of the "standard anelastic solid."[44]

In the present work we consider strain relaxation and internal friction experiments. The following initial conditions hold for strain relaxation:

$$\sigma = \sigma_o \text{ at } t = 0$$

$$\varepsilon = J_R \sigma_o \text{ at } t = 0$$

$$\sigma = \dot{\sigma} = 0 \text{ at } t > 0.$$

With the definition $\delta J \equiv J_R - J_U$ we obtain as a solution to Equation (1)

$$J(t) = \frac{\varepsilon(t)}{\sigma_o} = \delta J e^{-t/\tau_\sigma} \qquad (2)$$

for the relaxation of the compliance. The strength of the relaxation may be written

$$\Delta \equiv \frac{\delta J}{J_U} . \qquad (3)$$

In dynamic (internal friction) experiments, anelastic behavior appears as a phase lag ϕ of the strain behind the applied stress. In complex notation the periodic stress and strain are

$$\sigma = \sigma_o e^{i\omega t} \qquad (4)$$

and

$$\varepsilon = \varepsilon_o e^{i(\omega t - \phi)} . \qquad (5)$$

The strain may be decomposed into an in-phase and a quadrature component

$$\varepsilon = (\varepsilon_1 - i\varepsilon_2) e^{i\omega t} . \qquad (6)$$

Similarly the compliance J may be written in component form

$$J = J_1 + iJ_2 . \qquad (7)$$

The expressions for J_1 and J_2 are known as the Debye equations, and they are obtained from substitution of Equations (4) and (6) into Equation (1)

$$J_1 = J_U + \frac{\delta J}{1 + \omega^2 \tau_\sigma^2} \tag{8}$$

$$J_2 = \delta J \frac{\omega \tau_\sigma}{1 + \omega^2 \tau_\sigma^2} . \tag{9}$$

The internal friction is proportional to the ratio of the energy lost per cycle over the energy stored per cycle. This ratio is just J_2/J_1 which, from the decomposition of the compliance J, is tan ϕ. Therefore we find, for $\phi << 1$, the internal friction

$$\phi = \Delta \frac{\omega \tau}{1 + \omega^2 \tau^2} \tag{10}$$

where the subscript to τ has been omitted under the condition $\Delta << 1$. Equation (10) describes a symmetric peak in ϕ as a function of log $\omega\tau$. The peak maximum is found at log $\omega\tau = 0$, i.e., $\omega\tau = 1$, and its magnitude is $\Delta/2$. The existence of a functional dependence of τ upon temperature allows the measurement of ϕ as a function of temperature at fixed frequency.

For the case of uniaxial stresses applied to single crystals the appropriate elastic compliance is

$$J = \frac{s' + s''}{3} - (s' - s)\Gamma \tag{11}$$

where s is the compliance for a shear stress applied in the [010] direction across the (100) plane; s' is the compliance for a shear stress applied in the [1$\bar{1}$0] direction across the

(110) plane; and s" is one-third the hydrostatic compressibility. In terms of the three independent compliances of cubic crystals s_{11}, s_{12}, and s_{44} we have

$$s = s_{44}$$

$$s' = 2(s_{11} - s_{12})$$

$$s'' = s_{11} + 2s_{12} .$$

Γ is the orientation factor

$$\Gamma = \alpha_1^2\alpha_2^2 + \alpha_1^2\alpha_3^2 + \alpha_2^2\alpha_3^2 \qquad (12)$$

where the α_i are direction cosines between the stress direction and the cube axes.

3.2 Thermodynamics of Relaxation

The theory of the anelastic relaxation strength Δ (or δJ) has been worked out in detail by Nowick and Heller[45,46] and Nowick.[47] The theory is based upon the concept of the elastic dipole and upon the point symmetry of the defect which generates the elastic dipole. The point symmetry of a defect is the set of point group operations common to the defect in free space and to the site of the defect in the host lattice. The elements of the elastic dipole tensor may be defined as

$$\lambda_{ij}^{(p)} = \frac{\delta\varepsilon_{ij}}{\delta C_p} . \qquad (13)$$

Thus the elastic dipole or λ tensor element is the amount of strain introduced when unit concentration of defects orders into the p-th crystallographically equivalent orientation.

Under equilibrium conditions with no applied stress all of the n_t equivalent orientations of the defect (that can be distinguished by a stress field) have equal occupation probability. If C_o is the total concentration of defects which cause relaxation, then C_o/n_t is the equilibrium concentration in each orientation. With C_p the instantaneous concentration in the p-th sites, the total strain (elastic plus anelastic) may be written

$$\varepsilon = J_U\sigma + \sum_{p=1}^{n_t} \lambda^{(p)} \left(C_p - \frac{C_o}{n_t}\right) \tag{14}$$

where the strain indices have been dropped and it has been assumed that there are no interactions among the defects. The quantity $C_p - C_o/n_t$ is obtained by minimizing the free energy of the strained crystal containing defects, and the result is

$$C_p - \frac{C_o}{n_t} = \frac{C_o v_o \sigma}{n_t kT} \left[\lambda^{(p)} - \frac{1}{n_t} \sum_{p=1}^{n_t} \lambda^{(p)}\right] \tag{15}$$

where v_o is the molecular volume of the crystal. The relaxation of the compliance, δJ, is then obtained by substituting Equation (14) into Equation (13) and dividing by σ

$$\delta J = \frac{C_o v_o}{n_t kT} \left[\sum_p (\lambda^{(p)})^2 - \frac{1}{n_t} \left(\sum \lambda^{(p)}\right)^2\right] \tag{16}$$

which is valid for any stress. In the absence of a hydrostatic stress component the second term within the square brackets vanishes.

The procedure for identifying and analyzing unknown defect symmetries from relaxation data has been systematized by Nowick and Heller,[46] who used group representation theory to simplify the relationships among stress, compliance, and defect point symmetry. This simplification led to the establishment of selection rules which list the symmetries that can cause the relaxation of the various elastic compliances. Table I shows the rules for the relaxation of s, s', and s" in cubic crystals. An entry of zero means the relaxation is impossible, while the nonzero integers represent the number of relaxation processes (i.e., times) associated with the reorientation of the particular defect. With the aid of Equations (11) and (12) the table reveals the defect symmetries that may reorient under an applied uniaxial stress. In order that s" relax, the defect must undergo a change of volume due to the action of a hydrostatic stress component. The volume change can arise from a conversion (or reaction) of the defect into another defect of different point symmetry and volume.

As seen in Equation (16) the relaxation strength is proportional to the concentration of defects, C_o. If the relaxation is caused by a multiple atom defect, C_o will be the concentration of such defects in equilibrium with single atoms of the constituent elements (and with smaller clusters if

Table I

Selection Rules for Anelastic Relaxation

Compliance	Cubic	Tetragonal	Trigonal	Orthorhombic ⟨100⟩	Orthorhombic ⟨110⟩	Monoclinic ⟨100⟩	Monoclinic ⟨110⟩	Triclinic
s	0	0	1	0	1	1	2	3
s'	0	1	0	2	1	2	1	2
s"	1	1	1	1	1	1	1	1

necessary). In the case of hydrogen-impurity pairs (e.g., H-O or H-N) the following reaction obtains:

$$H + I \leftrightarrows H - I$$

The concentrations of free, or unpaired, impurity atoms, C_I, of free hydrogen atoms, C_H, and of H-I pairs obey the following equations at all temperatures:

$$C_{H-I} = \frac{z}{\beta} C_H C_I \, e^{B/kT} \tag{17}$$

$$C_H^T = C_H + C_{H-I} \tag{18}$$

$$C_I^T = C_I + C_{H-I} \, . \tag{19}$$

B is the binding enthalpy of the pair, and C_H^T and C_I^T are the total concentrations of hydrogen and impurity atoms, respectively. As expressed by Pfeiffer and Wipf[42] the constant β is the number of free sites for hydrogen occupation per solvent atom (the reduction in β due to impurity atoms being ignored) and the constant z is the number of trapping sites around each impurity. Thus β and z depend upon the symmetry and geometry of the H-I pairs and of the solvent lattice. The simultaneous solution of Equations (17) through (19), under the boundary condition $0 \leq C_I \leq C_I^T - C_H^T$ for $C_I^T > C_H^T$, yields

$$C_{H-I} = \frac{1}{2} \{C_H^T + C_I^T + \frac{\beta}{z} e^{-B/kT} - [(C_H^T + C_I^T + \frac{\beta}{z} e^{-B/kT})^2 - 4C_H^T C_I^T]^{\frac{1}{2}}\} \tag{20}$$

In the high temperature region C_{H-I} is given by Equation (17) with $C_H \simeq C_H^T$ and $C_I \simeq C_I^T$, while in the low temperature limit all the hydrogen atoms are trapped, and $C_{H-I} = C_H^T$.

3.3 Kinetics of Relaxation

The reciprocals of the relaxation times referred to in Table I may be expressed in terms of the rates of reorientation, ν_{1q}, from the p = 1 site of a defect to the qth member of its $n_t - 1$ other sites. The site numbering convention used by Nowick[48] is illustrated in Figure 2 where the defining principal axes of the strain tensors representing five defect symmetries are plotted in stereographic projection. No diagram is shown in Figure 2 for the ⟨100⟩ orthorhombic defect. The principal axes of this defect are aligned in the [100], [010], and [001] directions and are labelled a, b, and c. The numbering system is obtained by permutation of the principal axes in order among the allowed directions as follows: 1, abc; 2, acb; 3, bca; 4, bac; 5, cab; and 6, cba. The reorientation rates ν_{1q} for a particular defect symmetry are not all independent. Those sites whose defining principal axes have the same direction cosines with respect to the principal axis of the 1st site have identical reorientation rates from the 1st site. Table II lists the reorientation rates and the equalities among them for all of the possible defect symmetries in cubic crystals with the exception of the triclinic. By means of group representation theory Nowick[48] has obtained expressions for the reciprocal

Figure 2. The numbering system for defects in cubic crystals showing the allowed orientations of a principal axis of the defect in [001] standard stereographic projection.
After Nowick (48).

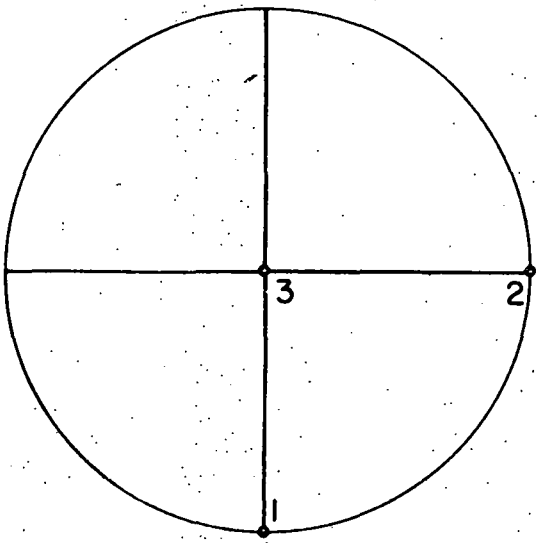

TETRAGONAL

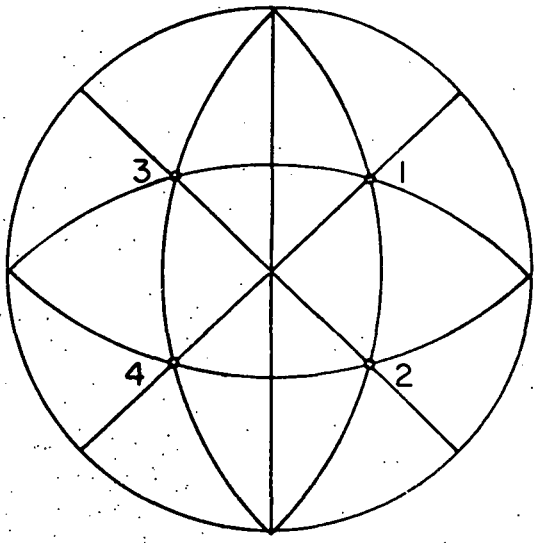

TRIGONAL

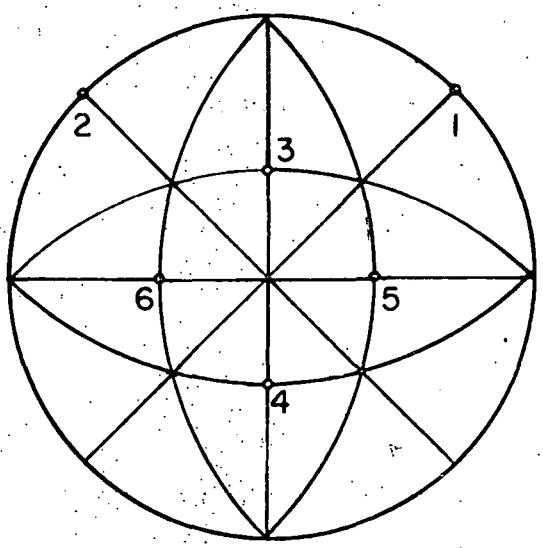

⟨110⟩ ORTHORHOMBIC

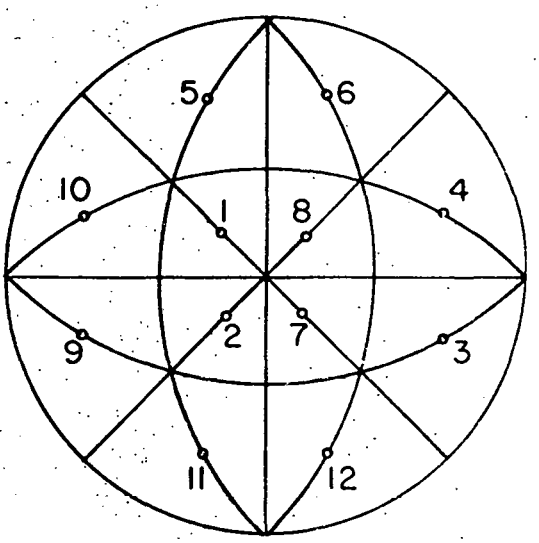

⟨110⟩ MONOCLINIC
⟨11U⟩

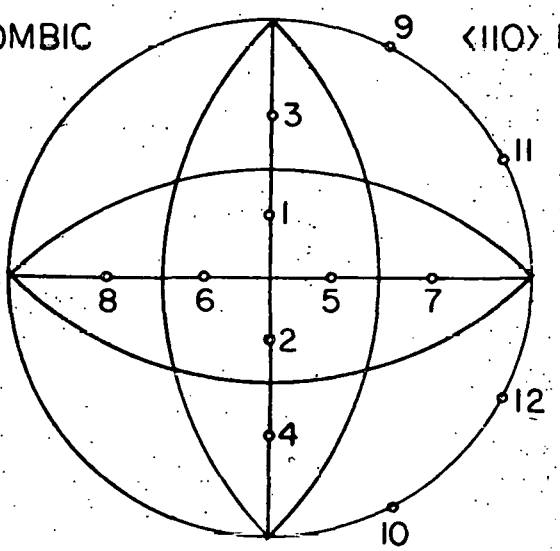

⟨100⟩ MONOCLINIC
⟨01U⟩

Table II

Reorientation Rates of Defect Symmetries in Cubic Crystals

Symmetry	Reorientation Rates
Tetragonal	$\nu_{12} = \nu_{13}$
Trigonal	$\nu_{12} = \nu_{13} = \nu_{14}$
⟨100⟩ Orthorhombic	$\nu_{12}, \nu_{14}, \nu_{16}$ $\nu_{13} = \nu_{15}$
⟨110⟩ Orthorhombic	ν_{12} $\nu_{13} = \nu_{14} = \nu_{15} = \nu_{16}$
⟨100⟩ Monoclinic	$\nu_{12}, \nu_{13}, \nu_{14}$ $\nu_{15} = \nu_{16}, \nu_{111} = \nu_{112}$ $\nu_{17} = \nu_{18} = \nu_{19} = \nu_{110}$
⟨110⟩ Monoclinic	$\nu_{12} = \nu_{18}$ $\nu_{13} = \nu_{14} = \nu_{111} = \nu_{112}$ $\nu_{15} = \nu_{110}, \nu_{16} = \nu_{19}$

relaxation times, in terms of the independent ν_{1q}'s of the various defects, for relaxations of the shear compliances s and s'. These expressions are listed in Table III. To complete the specification of an anelastic relaxation, the reorientation rates must be converted to the jump frequencies of the atoms comprising the defect: this procedure follows from inspection of the model of the defect in its host crystal.

Classical theory of thermally activated processes predicts that the relaxation time varies with temperature according to an Arrhenius equation:

$$\tau^{-1} = \tau_o^{-1} e^{-\Delta H/kT} \qquad (21)$$

where ΔH is the activation enthalpy (i.e., the height of the potential barrier between initial and final sites) and τ_o^{-1} is the product of a geometric constant, the vibration frequency of the mobile defect in its interstitial site, and an entropy factor.[49] Because of the concern (which has since been justified experimentally) that Equation (21) could not describe light interstitial diffusion at low temperatures, a number of quantum theories of diffusion have been devised. Two that will be mentioned here are those of Sussmann[50] and of Flynn and Stoneham.[22] These approaches share several physical ideas,[51] but are mutually exclusive in their proposals of dominant mechanisms. In Sussmann's theory the localized hydrogen atom is excited from its ground state to a band state by absorption

Table III

Relaxation Times of Defect Symmetries in Cubic Crystals

Symmetry	Compliance	τ^{-1}
Tetragonal	s′	$3\nu_{12}$
Trigonal	s	$4\nu_{12}$
⟨100⟩ Orthorhombic	s′	$(\nu_{12}+3\nu_{13}+\nu_{14}+\nu_{16})$ $\pm(\nu_{12}^2+\nu_{14}^2+\nu_{16}^2-\nu_{12}\nu_{14}-\nu_{12}\nu_{16}-\nu_{14}\nu_{16})^{\frac{1}{2}}$
⟨110⟩ Orthorhombic	s	$2\nu_{12}+4\nu_{13}$
	s′	$6\nu_{13}$

Table III continued

Symmetry	Compliance	τ^{-1}
⟨100⟩ Monoclinic	s	$2(\nu_{12}+\nu_{14}+\nu_{15}+\nu_{17}+\nu_{111})$
	s′	$(\nu_{13}+\nu_{14}+2\nu_{15}+6\nu_{17}+2\nu_{111})$
		$\pm[(\nu_{15}+\nu_{111}-\nu_{13}-\nu_{14})^2+3(\nu_{15}+\nu_{111})^2]^{\frac{1}{2}}$
⟨110⟩ Monoclinic	s	$(6\nu_{12}+5\nu_{13}+\frac{3}{2}\nu_{15}+\frac{3}{2}\nu_{16}+\nu_{17})$
		$\pm[(\nu_{12}-\nu_{13}-\nu_{17}+\frac{1}{2}\nu_{15}+\frac{1}{2}\nu_{16})^2+2(\nu_{15}-\nu_{16})^2]^{\frac{1}{2}}$
	s′	$6\nu_{13}+3\nu_{15}+3\nu_{16}$

of a phonon of energy E. Within the band the atom reorients or diffuses rapidly and then decays to the ground state of an adjacent site by emission of a phonon. The jump frequency is controlled by the rate of excitation to the band and is proportional to $e^{-E/kT}$. Multiphonon-assisted tunnelling is considered insignificant in this theory.

Hydrogen is viewed as being self-trapped, in the theory of Flynn and Stoneham, because of strong interactions between it and neighboring host atoms. Only at impractically low temperatures is diffusion through a band predicted. Experimentally detectable motion of hydrogen occurs by tunnelling when lattice fluctuations render the initial and final sites of the atom energetically equivalent; hence the diffusion is called "lattice-activated." The activation energy, E_a, is the strain energy required to bring about this energetic equivalence,[52] and it is related to the elastic dipole tensor (and thus the volume of solution) of the defect. The hopping rate is proportional to the square of the transition matrix $J_{pp'}$, which is given by

$$J_{pp'} = \langle \phi_p | H_{int} | \phi_{p'} \rangle \qquad (22)$$

where ϕ_p and $\phi_{p'}$ are the orthogonal interstitial impurity wave functions at site p and site p', respectively, and where H_{int} represents the interaction between the impurity and the lattice.

At low temperatures ($T << \theta_D/2$) the hopping rate is determined by a two-phonon process, and

$$\frac{1}{\tau} = 57600\ \pi\omega_D \frac{|J_{pp'}|^2}{(\hbar\omega_D)^4} E_a^2\ e^{-5E_a/\hbar\omega_D} \left(\frac{T}{\theta_D}\right)^7 . \qquad (23)$$

ω_D and θ_D are the Debye frequency and temperature, respectively. At high temperatures ($T >> \theta_D/2$) a many-phonon process activates diffusion, and the hopping rate is given by

$$\frac{1}{\tau} = \left(\frac{\pi}{4\hbar^2 E_a kT}\right)^{1/2} |J_{pp'}|^2\ e^{-E_a/kT} . \qquad (24)$$

The hopping rate at any temperature T is given by[53]

$$\frac{1}{\tau} = \frac{|J_{pp'}|^2}{\hbar k\theta_D} \exp(-f) \int_{-\infty}^{\infty} dt(\exp g - 1) \qquad (25)$$

where

$$f(a) = \gamma \int_0^1 dx\ x^3 \coth(ax) \qquad (26)$$

and

$$g(a,t) = \gamma \int_0^1 dx\ x^3\ \mathrm{cosech}(ax) \cos(xt) \qquad (27)$$

with the parameters $a \equiv \theta_D/2T$, and $\gamma \equiv 20E_a/k\theta_D$.

4. EXPERIMENTAL PROCEDURE

4.1 Specimen Preparation

4.1.1 Single crystal Nb-O-H specimens

In measurements of high frequency ultrasonic attenuation it is desirable to use large diameter transducers so that the stress waves injected into the sample are planar, and to have a large ratio of sample to transducer diameter in order to reduce the contribution of reflections of waves from sample surfaces not parallel to the transducer.[54] This method of measurement requires large single crystals of niobium which were grown by the method of strain anneal described by Digges and Achter.[55] The starting material was a twelve-inch length of one-inch diameter niobium rod supplied by Wah Chang Albany Corporation. The material was 95% recrystallized, and it contained several hundred appm substitutional impurities, primarily tantalum, tungsten, zirconium, and molybdenum, as shown in Table IV.

The strain anneal technique as used in this work consisted of a recrystallization anneal at 1600°C of the as-received rod, followed by an axial strain of 2% in compression and then by a growth anneal at 2200°C. Heating of the rod was achieved by lowering it at a controlled rate through an induction coil in a diffusion-pumped vacuum system. A given section of the rod was maintained at temperature for approximately one hour in

Table IV

Mass Spectrographic Analysis* of Nb Single Crystals

Element	Concentration (appm)	Element	Concentration (appm)
Pb	0.1	Cu	≤ 0.04
Au	≤ 0.08	Ni	0.04
Re	< 0.08	Fe	0.05
W	0.8	Mn	≤ 0.03
Ta	200	Cr	≤ 0.04
Sb	≤ 0.1	V	≤ 0.03
In	< 0.3	Ti	≤ 0.04
Mo	≤ 0.1	Ca	3
Zr	< 0.06	K	2
Se	2	Cl	< 9
As	< 0.03	Si	3
Zn	≤ 0.06	Al	0.2
Mg	1	Na	< 1

*This analysis is semiquantitative with an accuracy of ÷/× a factor of three.

the recrystallization step and ten hours in the growth step. During the recrystallization anneal a partial pressure of oxygen of 2×10^{-5} torr was introduced into the vacuum system to oxidize and degas carbon impurities; the final growth anneal was performed in a vacuum of 5×10^{-6} torr.

After the first anneal visual examination of the surface of the rod revealed a grain size of 1 to 3 mm. The growth anneal produced three large grains of 2, 3, and 4½ in. in length which extended across the diameter of the rod. Determination of the grain structure was made by back-reflection Laue x-ray photographs. Grain boundaries were found to be nearly perpendicular to the rod's axis.

Three single crystal specimens were cut from two of the large grains by spark discharge machining. Orientation within about ± 1° of the desired crystallographic directions was made by the back-reflection Laue technique. Specimens 1 and 3 had two parallel faces cut perpendicular to a ⟨111⟩ direction; specimen 2 had one pair of faces cut perpendicular to a ⟨100⟩ direction and another pair perpendicular to a ⟨110⟩ direction 90° away from the selected ⟨100⟩. After spark machining, the specimens were etched to remove surface damage and contamination using the standard niobium etchant of 1:1:1 by volume of concentrated hydrofluoric acid:nitric acid:lactic acid.

Interstitial impurities were removed from the specimens by degassing at high temperatures in an ultra-high vacuum system, by means of electron beam heating. Specimens 1 and 2 were

outgassed together at 2000°C and 4.2 x 10^{-10} torr for 2½ hours, and specimen 3 was held at 2100°C and 3 x 10^{-10} torr for 5½ hours. The desired oxygen concentration was obtained by annealing at 1900°C in the partial pressure of oxygen prescribed by the steady-state data of Fromm and Jehn.[56] Specimens were held at temperature for at least 17 hours to ensure a homogeneous interstitial concentration.

Before hydrogen was introduced, the specimens were hand polished to make the faces as flat and parallel as possible. Throughout the process the specimens were mounted in wax at the centers of three-inch diameter aluminum polishing holders. Shaping and rough polishing were performed on 400 and 600 grit silicon carbide paper. Intermediate polishing was done on an Ablap diamond impregnated disc with about 11μ particle size and on a granite flat using 15μ SiC powder. Final polishing was also done on granite flats using 6μ and 3μ Al_2O_3. The quality of flatness and parallelism was gauged with a Johansen Mikrokator, and a deviation of less than 10^{-5} in./in. in planarity and parallelism was achieved.

The concluding step in the preparation was the alloying of the specimens with hydrogen. Whereas useful concentrations of heavy interstitials in solid solution may be quenched into niobium from the equilibrium or steady-state conditions, the high diffusivity of hydrogen in niobium precludes this. During the alloying with hydrogen "iso-concentration" lines, derived from the solubility data of Velekis,[57] were followed by

adjusting the hydrogen pressure as the specimen was slowly cooled from the temperature of initial equilibration. That temperature was 650 or 700°C, chosen so that the impermeable oxide on the specimen surface would dissolve into the metal and allow hydrogen to diffuse in. The hydrogen gas was purified by diffusion through a Pd-Ag membrane, and the alloying procedure was carried out in a stainless steel, turbo-molecular pumped system. At the end of the slow cooling (about 150°C), air was admitted briefly into the system to reoxidize the niobium surface and so confine the hydrogen within the specimen. Table V lists the concentrations of the various interstitial solutes after specimen preparation. Determination of the hydrogen concentration was made by a vacuum extraction method, while the other elements were assayed with a vacuum fusion technique.

4.1.2 Polycrystalline sheet specimens

Rectangular polycrystalline sheet specimens were employed in strain relaxation and low frequency internal friction experiments. The specimens were cut from 76μ and 178μ thick niobium stock supplied by Wah Chang and were outgassed and nitrogen alloyed in a U.H.V. system. Strips 14 mm in width and of various lengths were outgassed for one hour at 1900°C and 2×10^{-10} torr. Doping with high-purity nitrogen was carried out immediately after outgassing by equilibration with 2.2×10^{-5} torr of N_2 gas at 1700°C for one hour.[58] These times were chosen to allow equilibration of the specimen with the gaseous atmosphere.

Table V

Interstitial Concentrations of Nb Specimens

Specimen	Condition	Concentration (at.%)			
		H	C	N	O
1	Single Crystal	0.23	---	0.048	0.56
2	Single Crystal	0.22	---	0.048	0.56
3	Single Crystal	0.34	0.014	0.061	0.49
5	Polycrystalline	0.41	---	0.39	0.0061
7	Polycrystalline	0.46	---	0.57	0.018

Hydrogen was introduced into the specimens by cathodic charging at room temperature in a solution of 0.1% by weight H_2SO_4 in deionized water.[42] A coil of platinum wire was used for the anode, and the current density was about 60 ma/cm^2. The uptake of hydrogen into the specimen was monitored periodically during charging by measuring the change in resistance. A value of 15 μΩ-cm was taken as the value of the resistivity of the Nb-N alloy at room temperature; the value used for the resistivity increment due to hydrogen was 0.75 μΩ-cm/at.%.[10] The measured interstitial concentrations of the Nb-N-H specimens are also listed in Table V.

4.2 Methods of Measurement

4.2.1 Ultrasonic attenuation in Nb-O-H single crystals

The pulse-echo technique of attenuation measurement was used to study the internal friction in the three Nb-O-H single crystals. Figure 3 shows a block diagram of the commercially available electronic equipment employed in this work. Pulses of very-high frequency (30-170 MHz) were sent from a Matec Model 6000 pulse generator and receiver to an x-cut quartz transducer bonded by epoxy to one of the polished faces of the specimen. The transducers were usually 3/8" in diameter with a 10 MHz resonance frequency, although a 1/4" 7 MHz type also was used. The transducer, driven at an odd multiple of its resonance frequency, injected longitudinal stress waves into the specimen, and converted the echoes into electrical signals

Figure 3. Block diagram of the vhf pulse-echo internal friction equipment.

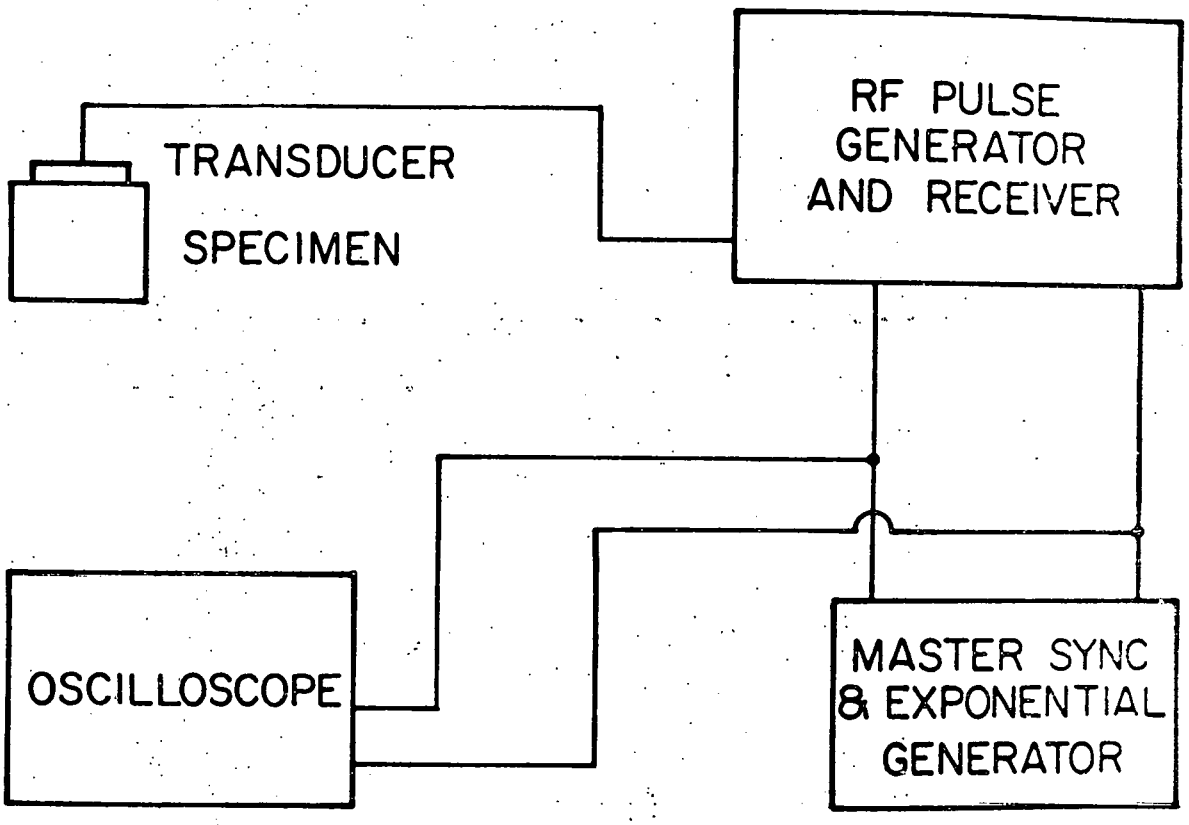
RF PULSE
GENERATOR
AND RECEIVER
TRANSDUCER
SPECIMEN
OSCILLOSCOPE
MASTER SYNC
& EXPONENTIAL
GENERATOR

whose amplitudes were displayed on an oscilloscope. The attenuation experienced by the stress wave pulse was measured by carefully superimposing a calibrated exponential decay curve (from a Matec Model 1204) on the echo train. The decay constant, α, of the exponential curve was read directly from the Model 1204, in units of db/μsec.

Attenuation was measured between 110 and 300K at various fixed frequencies. The specimens were placed inside a small liquid nitrogen cryostat whose temperature was lowered at the rate of 1K/min during the course of a run. Control of the cooling rate was achieved by balancing the heat output from an electrical resistance heater with cold nitrogen gas or liquid nitrogen. Temperature was measured with a copper constantan thermocouple in contact with the specimen, and the air inside the cryostat was displaced with He gas to produce a dry environment.

4.2.2 Low frequency internal friction in the Nb-N-H system

Low frequency (3-165 Hz) internal friction measurements were made on the Nb-N-H polycrystalline specimens. The configuration of the specimen (Figure 4) was that of a thin cantilever beam which was oscillated in a flexural mode at its resonance frequency. The resonance frequency is given by[44]

$$f_r = \frac{0.1615\ t}{\ell^2} \left(\frac{E}{\rho}\right)^{\frac{1}{2}} \qquad (28)$$

where E is the Young's modulus of the material, ρ the density,

Figure 4. Schematic diagram of the specimen configuration for the low frequency internal friction and the strain relaxation experiments.

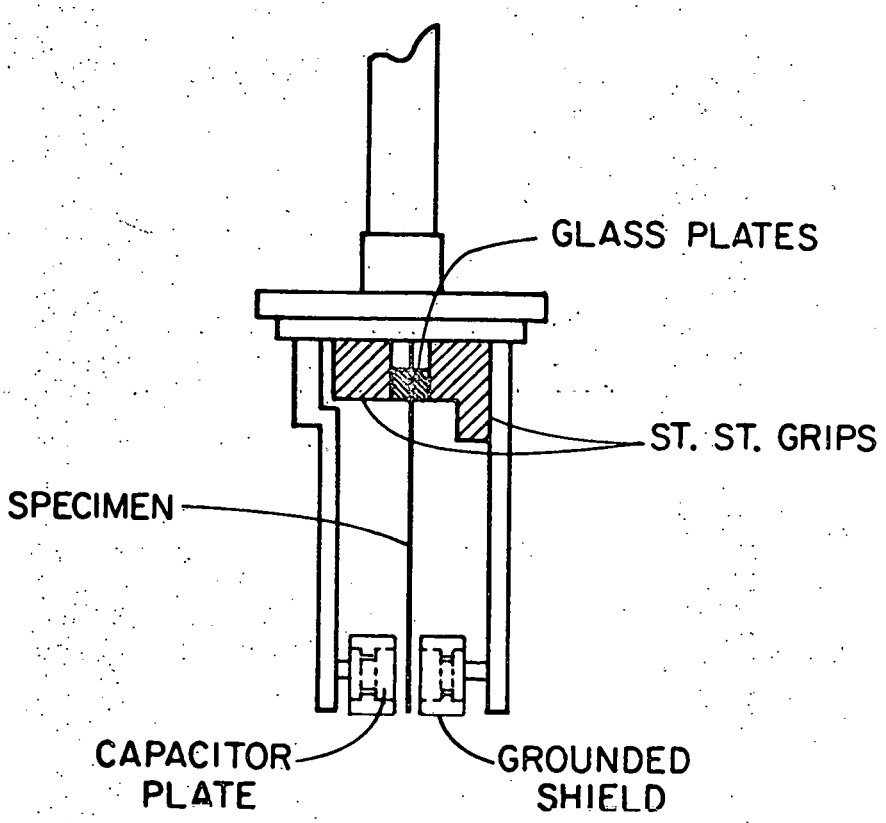
GLASS PLATES
ST. ST. GRIPS
SPECIMEN
CAPACITOR PLATE
GROUNDED SHIELD

and t and ℓ the thickness and length of the specimen, respectively. The two thicknesses of specimens thus provided two ranges of frequencies, particular values of which were obtained by cutting the specimen to the appropriate length. Additionally, lower frequencies (< 10 Hz) were obtained by attaching weights to the free end of a specimen. In these cases the specimens oscillated as an end-loaded cantilever beam whose frequency is given by[44]

$$f = \frac{0.1615\ t}{\ell^2} \left[\frac{E}{\rho}\left(1 + \frac{4m}{m_s}\right)\right]^{\frac{1}{2}} \qquad (29)$$

where m is the end mass and m_s is the specimen mass. The amplitude of vibration was chosen to give a large ratio of signal to noise (the latter mostly the result of extraneous vibrations) while ensuring only elastic strain of the specimens. In terms of the deflection, δ, and the dimensions t and ℓ, the maximum strain at the surfaces of the clamped end is given by

$$\varepsilon_{max} = \frac{3\delta t}{2\ell^2} . \qquad (30)$$

Strain values were typically 10^{-5} to 10^{-4}.

The manner of clamping the specimen was a critical experimental problem due to the contraction of materials upon cooling. It was found that, rather than squeezing the sample directly between stainless steel jaws, a more rigid and temperature insensitive grip was obtained when the specimen was held between pieces of microscope slide glass (one of which was silver

painted for electrical conductivity) which then were clamped by the metal jaws. Vitreous silica has little dimensional change when cooled from 273K to 100K, and this method of gripping resulted in an increased clamping force. Clamping of the thin specimens without the vitreous silica plates resulted in erratic changes of damping on cooling or heating.

Oscillation of the specimen and detection of the oscillation was achieved with biased parallel plate capacitors, one plate of which was the free end of the specimen. The other plates were stainless steel discs 1 cm in diameter located 0.5 to 3 mm from the specimen. The discs were biased 42.5 volts with respect to the specimen; typical drive voltages were 1 to 20 volts rms, while pick-up voltages were a few tenths of 1 mv. Internal friction peaks were recorded by measuring the drive voltage versus temperature at a constant amplitude of vibration, by measuring the amplitude at constant drive voltage, or by counting the number of oscillations of the specimen in a free decay between two fixed amplitudes.

In the first mode of measurement a Spectral Dynamics Model SD105B amplitude servo/monitor (Figure 5) adjusted the drive voltage to maintain the pick-up voltage, i.e., the amplitude of vibration, at a preset level. Driving at the specimen's resonance frequency was obtained by phase-locking a Hewlett Packard Model 3300A function generator (with a model 3302A trigger/phase lock plug-in) to the amplified pick-up signal. The phase angle between the pick-up signal and the sine wave output was

Figure 5. Block diagram of the low frequency internal friction equipment.

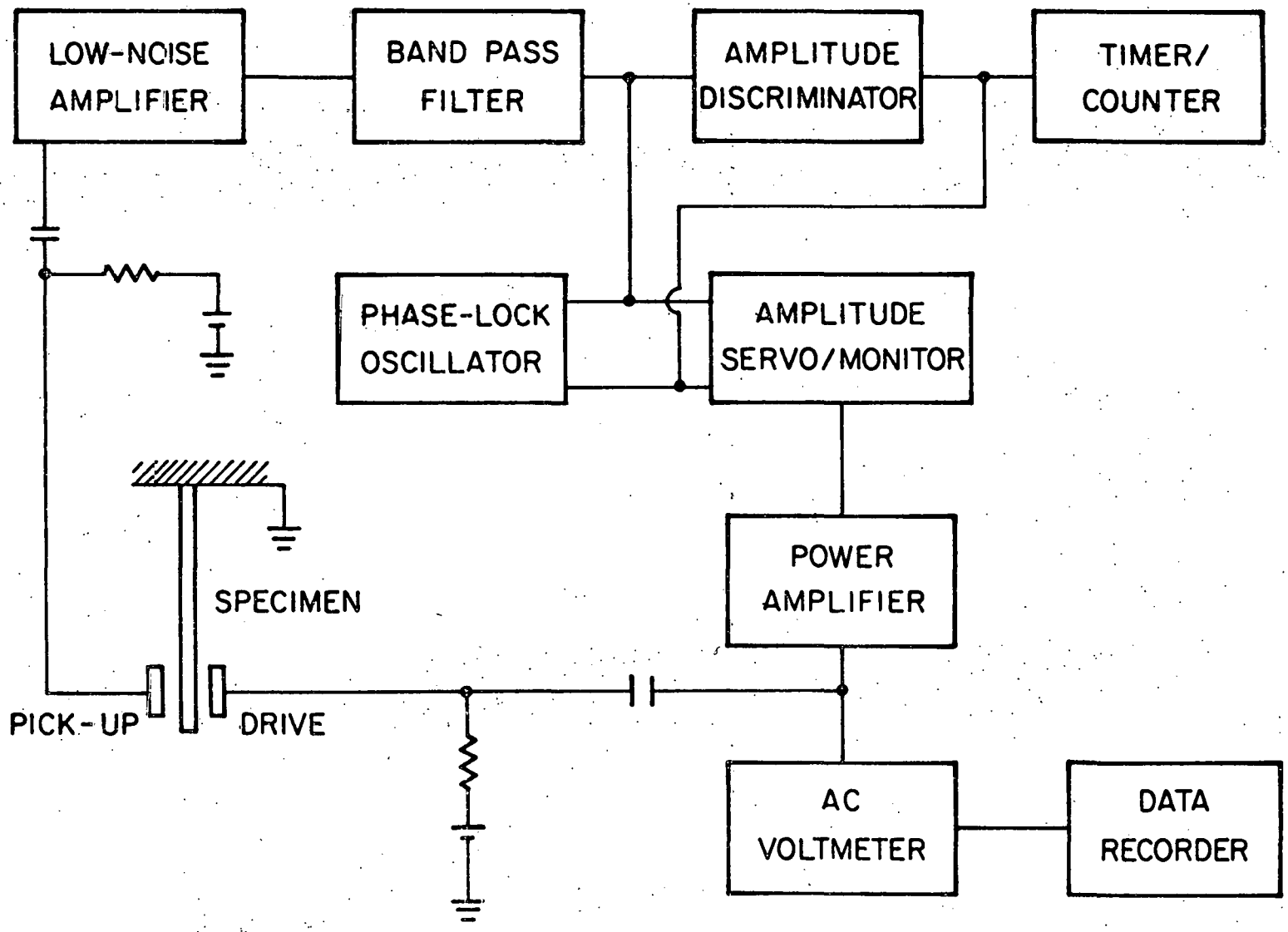
LOW-NOISE AMPLIFIER
BAND PASS FILTER
AMPLITUDE DISCRIMINATOR
TIMER/ COUNTER
PHASE-LOCK OSCILLATOR
AMPLITUDE SERVO/MONITOR
POWER AMPLIFIER
SPECIMEN
PICK-UP
DRIVE
AC VOLTMETER
DATA RECORDER

set to maximizé the ratio of pick-up voltage to drive voltage. This method of operation was satisfactory at frequencies above 9 Hz, but at lower frequencies the amplitude control loop became unstable, so that the alternatives mentioned above were used. Under constant drive voltage conditions, the pick-up voltage was measured as a function of temperature; as before, the frequency of the drive voltage was phase-locked to the pick-up signal. At the lowest frequency of measurement phase-locking to the pick-up signal was not possible with the available electronics; instead the specimen was manually excited to vibrate at its resonance frequency, and the oscillations during free decay were counted.

The clamped specimen and its pick-up and drive electrodes were enclosed by a copper and brass tube about which an electrical resistance heater was noninductively wound. This module was suspended inside a cylindrical stainless steel vacuum chamber which was located in a glass liquid helium dewar. The vacuum chamber was pumped mechanically to about 10^{-3} torr, with further pumping to about 10^{-4} torr when liquid helium was transferred into the dewar. Data were recorded during warming by ohmic heating from 10K at a rate $\leq$ 0.5 K/min. Temperature was measured by means of an Au-0.7%Fe versus chromel thermocouple attached to one of the stainless steel specimen clamps.

4.2.3 Strain relaxation in the Nb-N-H system

Measurements of the relaxation of the anelastic strain in Nb-N-H polycrystalline specimens were made at various

temperatures in the range 39 to 58K. The specimen was clamped as in Figure 4 except that the glass plates insulated the specimen from ground. The specimen and a single copper disc 1.5 cm in diameter formed a parallel plate capacitor whose capacitance was measured (Figure 6) with a General Radio Type 1615-A capacitance bridge, using a three-conductor method by which stray capacitances to ground were rejected. The capacitance bridge developed an output voltage proportional to the difference in capacitance between the equilibrium position and a deflected position of the specimen. An error of about 0.1 percent arose from taking the bridge output as directly proportional to the amount of deflection of the specimen. The bridge output was detected by a PAR Model 129 lock-in amplifier; a resolution of 1 μv was obtained which corresponded to a change in plate separation of about 0.2 μm.

The specimen was deflected elastically at its free end by an electromagnetically operated plunger from an initial, equilibrium spacing of about 0.7 mm to about 2.5 mm. The specimen, which was 178μ thick, 1.4 cm wide, and 5.5 cm long, experienced a maximum strain of about 10^{-4}. For the strain relaxation measurements the specimen was placed in a modified version of the liquid helium cryostat described in the previous section. To dampen transient vibrations, about 1 torr of helium gas was admitted to the experimental chamber. This gas proved to be such a good thermal link from the specimen to the liquid helium in which the experimental chamber was immersed that it was

Figure 6. Block diagram of the strain relaxation equipment.

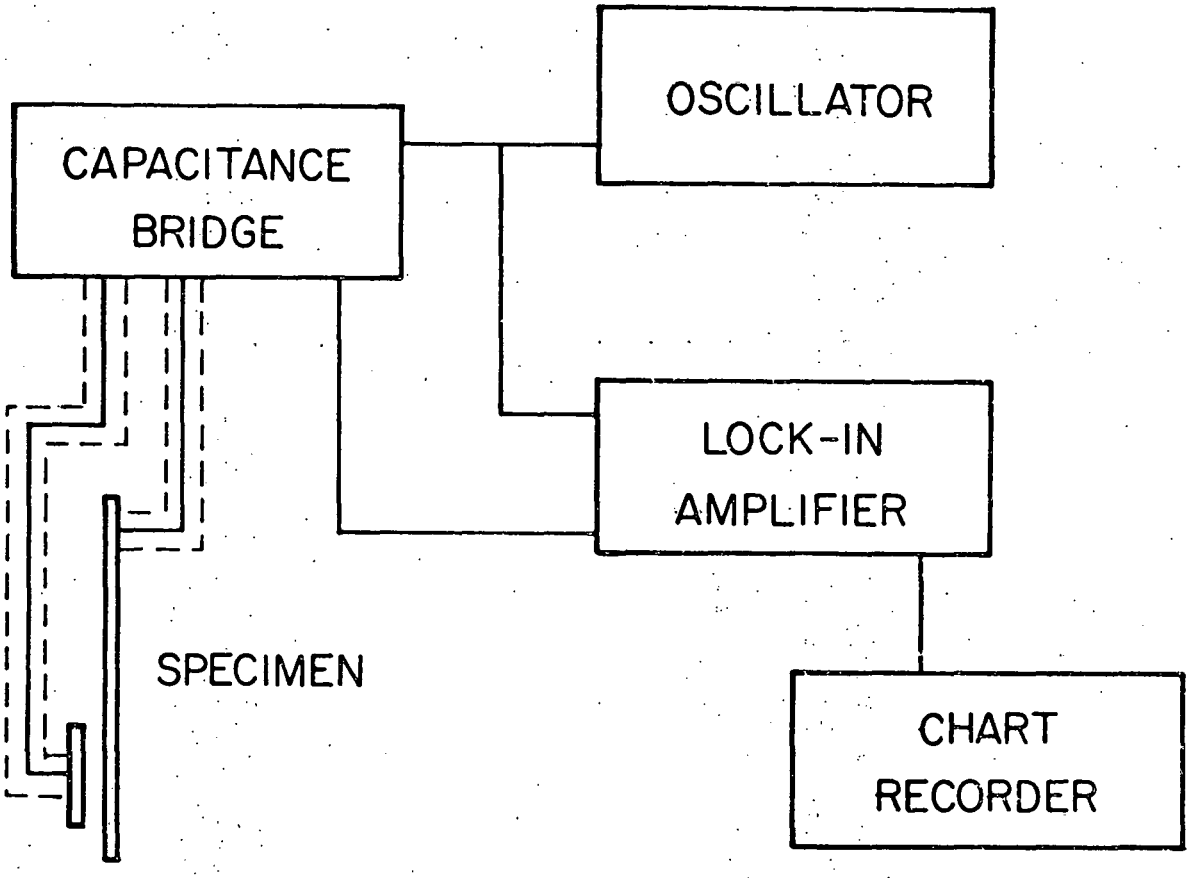
OSCILLATOR
CAPACITANCE BRIDGE
LOCK-IN AMPLIFIER
SPECIMEN
CHART RECORDER

necessary to insulate the chamber with a vacuum jacket. A very small partial pressure of helium was allowed in the jacket, the thermal conductivity of which was easily balanced by the specimen module heater to give the desired test temperature without excessive liquid helium consumption and without the electrical interference of high heater currents. The temperature, measured as before, was held constant to within 1/3K by manual control over the course of a relaxation.

5. RESULTS AND DISCUSSION

5.1 Internal Friction Due to O-H Pairs

Internal friction peaks were observed for longitudinal modes propagating in each of the three principal orientations of the Nb-O-H single crystals and at all measuring frequencies. No peaks were observed in the same specimens after hydrogen degassing, thus confirming that hydrogen is the mobile species responsible for these relaxations. Since the specimens were relatively rapidly cooled after oxygen doping and since the oxygen concentration exceeded that of hydrogen in all cases, it may be concluded that the hydrogen atoms were bound singly to individual oxygen atoms.[4] The internal friction (Q^{-1}) was measured as a function of temperature over a wide frequency range and was obtained from the exponential decay constant α by

$$Q^{-1} = \frac{\alpha}{2.72 \times 10^{-5} \nu}$$

where ν is the measuring frequency in Hz. Some representative results found with an applied stress frequency of 70 MHz are shown in Figures 7, 8, and 9 for the ⟨100⟩, ⟨110⟩, and ⟨111⟩ orientations, respectively. The peaks have been plotted as damping above background, where the background internal friction levels at all the measuring frequencies were relatively independent of temperature and had values in the range of

Figure 7. Internal friction versus temperature measured in the ⟨100⟩ direction at 70 MHz. The error bar shows the uncertainty in the data.

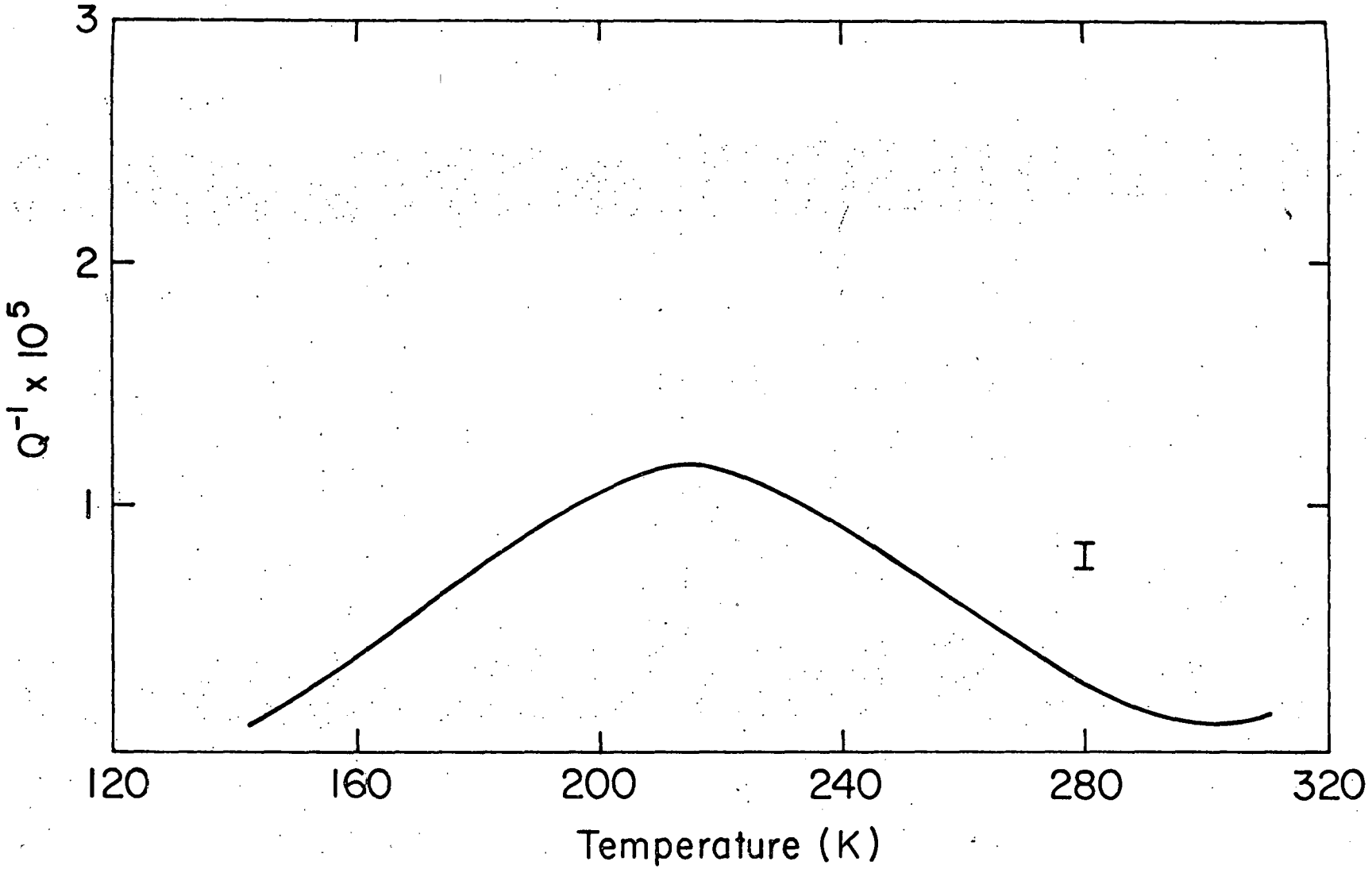
3
2
1
$Q^{-1} \times 10^5$
I
120
160
200
240
280
320
Temperature (K)

Figure 8. Internal friction versus temperature measured in the ⟨110⟩ direction at 70 MHz. The error bar shows the uncertainty in the data.

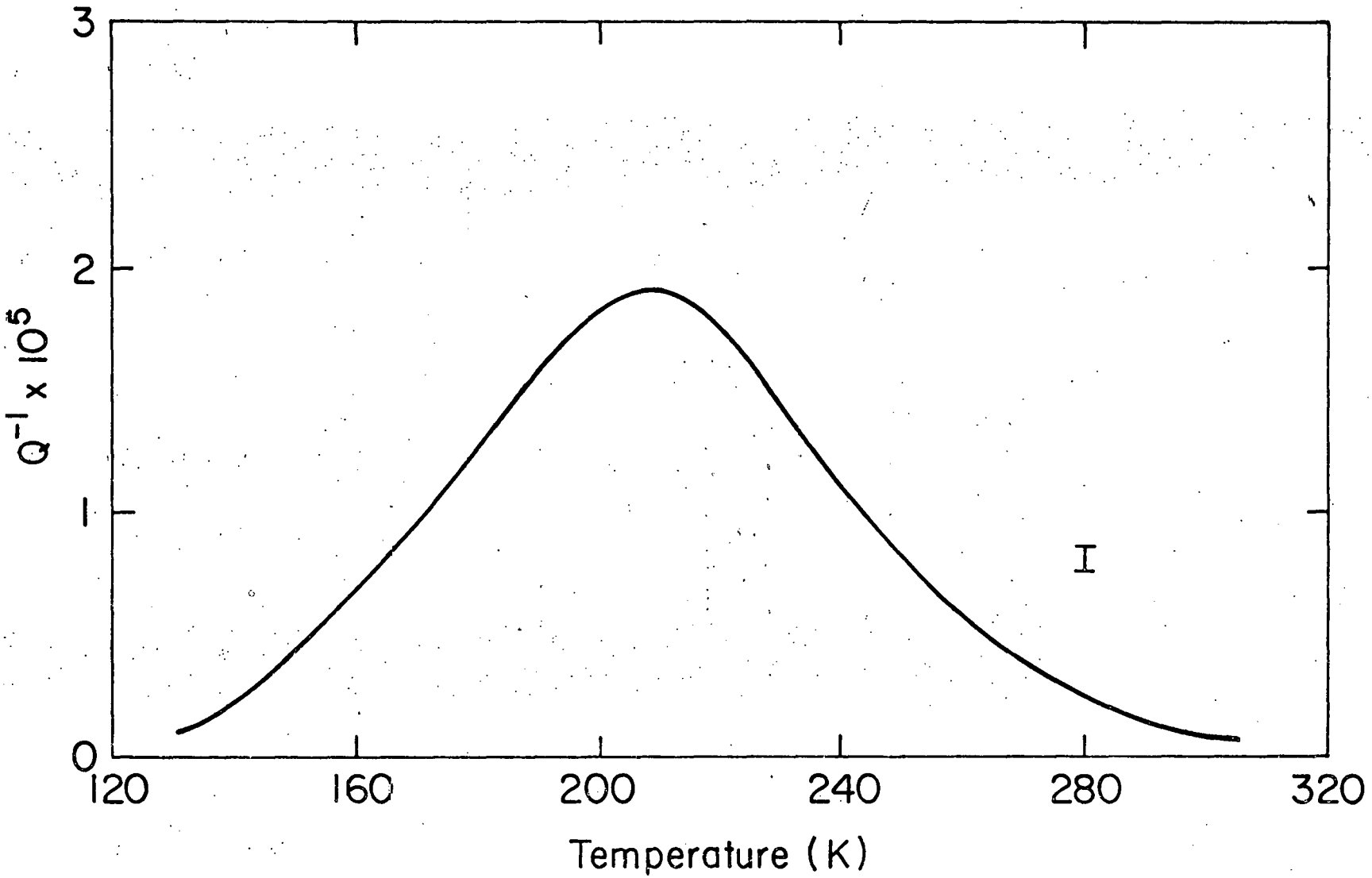
3
2
1
0
$Q^{-1} \times 10^5$
120
160
200
240
280
320
Temperature (K)
I

Figure 9. Internal friction versus temperature measured in the ⟨111⟩ direction at 70 MHz. The error bar shows the uncertainty in the data.

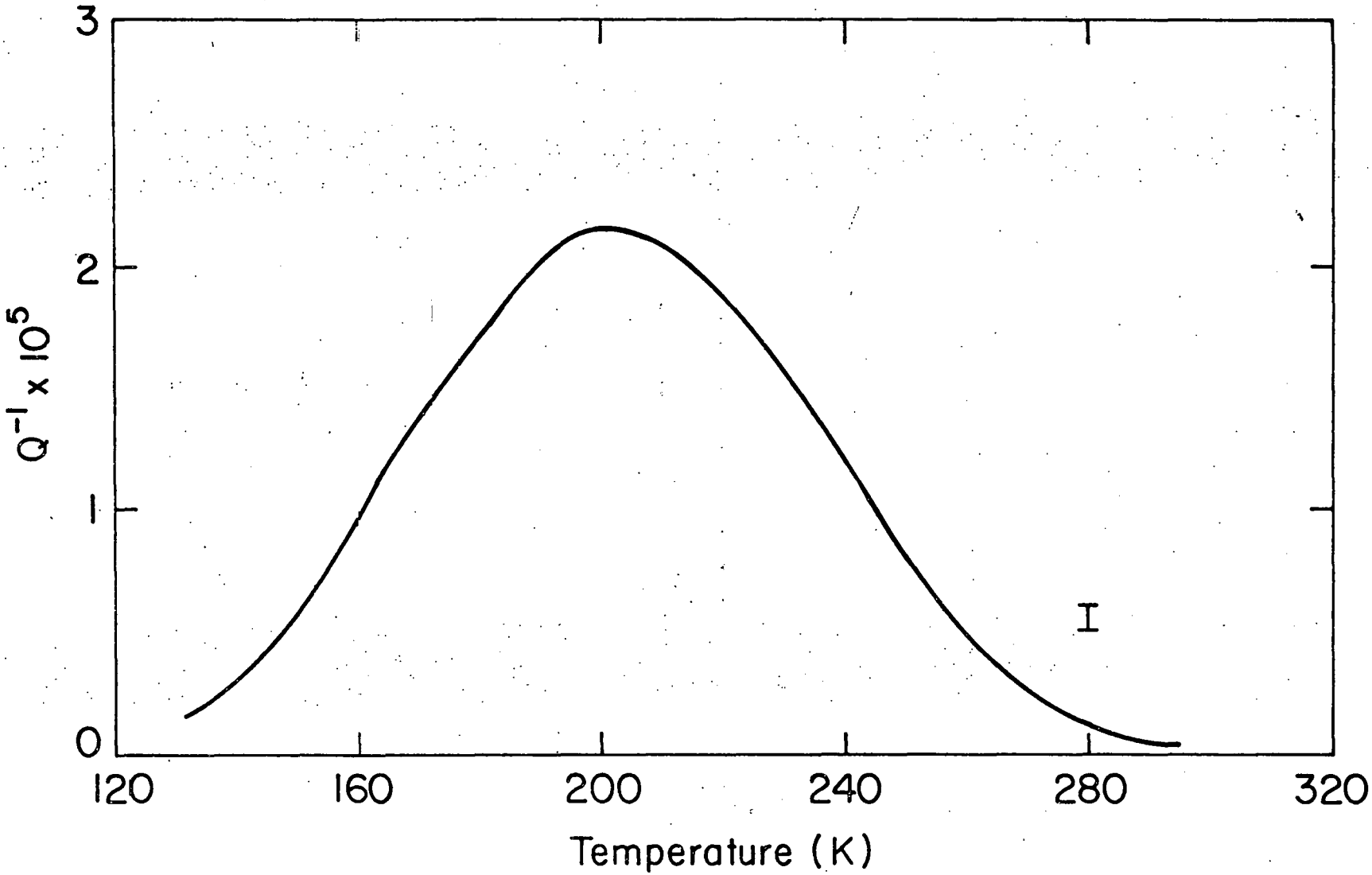
3
2
1
0
$Q^{-1} \times 10^5$
120
160
200
240
280
320
Temperature (K)
I

2×10^{-5} to 3×10^{-5} for specimens 2 (both ⟨100⟩ and ⟨110⟩) and 3, but ranged as high as 5×10^{-5} to 7×10^{-5} in specimen 1. (The high backgrounds in specimen 1 may have resulted from the reflection of the elastic stress waves from nonperpendicular sides of this specimen. The sides of specimens 2 and 3 were perpendicular to the quartz transducer.) The descriptive parameters of internal friction peaks are the temperature of maximum damping T_m, the peak height Q_m^{-1}, and the half-width in terms of reciprocal temperature $\Delta(T^{-1})$. These data are listed in Table VI for all the measured O-H internal friction peaks of this experiment. It can be clearly seen that the peak heights are quite small, seldom exceeding the background damping in amplitude.

In light of the condition $\omega\tau = 1$ for the peak maximum and of Equation (21), the log of the applied stress frequency has been plotted as a function of the corresponding reciprocal of T_m in Figures 10, 11, and 12 for the three orientations. As a first approximation a single relaxation process has been assumed for each orientation throughout the temperature range of the experiment. Therefore a least-squares fit of the data to the equation $\log \nu = \log \nu_o - \Delta H/kT$ was made and yielded the frequency factors and activation enthalpies shown in Table VII. The data of specimens 1 and 3 have been combined for this determination of ν_o and ΔH_1 since the jump frequency has been shown to be independent of hydrogen and oxygen concentration at these low solute levels.[4] The activation enthalpies are

Table VI

Summary of O-H Experimental Data

Specimen - Orientation	f (MHz)	T_m (K)	Q_m^{-1} x10^5	$\Delta(T^{-1})_{exp}$ (K^{-1})x10^3	$\frac{\Delta(T^{-1})_{exp}}{\Delta(T^{-1})_{th}}$
1 - ⟨111⟩	49	190 ± 3	2.4	2.4	1.3
	70	202 ± 4	2.2	2.1	1.1
	105	200 ± 3	0.86	1.3	0.7
$\Delta(T^{-1})_{th} = 1.9 \times 10^{-3}$	133	227 ± 4	1.4	1.8	0.9
	150	222 ± 4	1.3	1.8	0.9
3 - ⟨111⟩	50	197 ± 4	3.1	3.5	1.8
	70	199 ± 3	2.5	2.8	1.5
	90	205 ± 4	1.9	2.3	1.2
	110	215 ± 3	1.8	2.0	1.1
$\Delta(T^{-1})_{th} = 1.9 \times 10^{-3}$	130	220 ± 4	1.8	2.4	1.3
	150	223 ± 4	1.4	2.1	1.1
	170	224 ± 4	1.3	2.2	1.2

Table VI continued

Specimen - Orientation	f (MHz)	T_m (K)	Q_m^{-1} x10^5	$\Delta(T^{-1})_{exp}$ (K^{-1})x10^3	$\frac{\Delta(T^{-1})_{exp}}{\Delta(T^{-1})_{th}}$
2 - ⟨100⟩	30	195 ± 3	1.3	2.0	1.5
	50	201 ± 3	1.3	2.0	1.5
	70	215 ± 4	1.1	2.0	1.5
$\Delta(T^{-1})_{th} = 1.3 \times 10^{-3}$	110	216 ± 3	0.62	1.7	1.3
	130	223 ± 3	0.54	1.4	1.1
2 - ⟨110⟩	50	207 ± 5	2.6	2.0	2.4
	70	211 ± 4	1.8	1.8	2.1
	110	220 ± 5	1.2	1.8	2.1
$\Delta(T^{-1})_{th} = 8.4 \times 10^{-4}$	130	220 ± 4	1.3	1.9	2.3
	150	224 ± 4	2.2*	1.6	1.9
	170	220 ± 4	2.4*	1.8	2.1

*For these runs C_H^T = 0.48 a/o.

Figure 10. The logarithm of the measuring frequency versus the reciprocal of the internal friction peak temperature in the ⟨100⟩ direction.

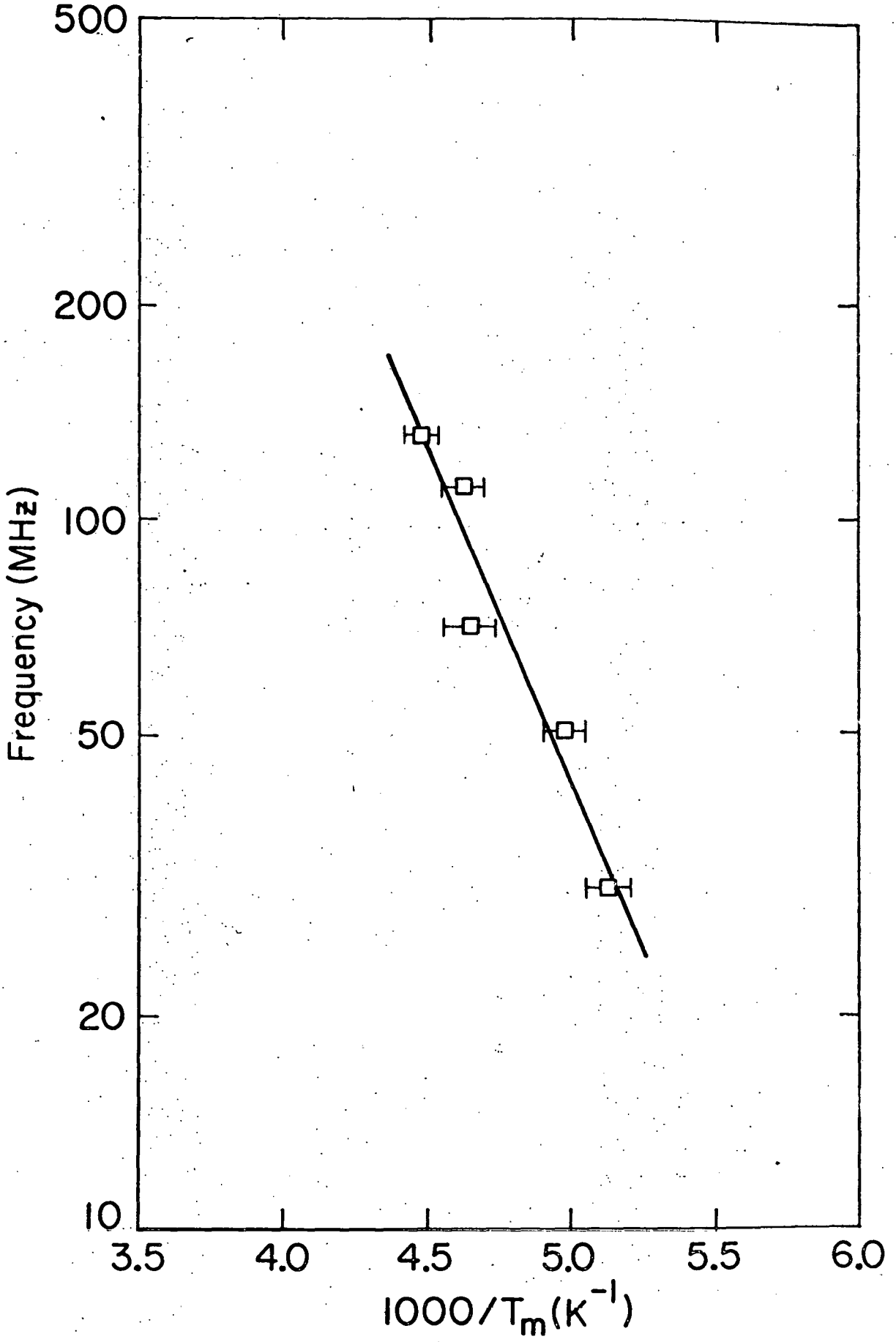
500
200
100
50
20
10
Frequency (MHz)
3.5
4.0
4.5
5.0
5.5
6.0
1000/T_m(K^-1)

Figure 11. The logarithm of the measuring frequency versus the reciprocal of the internal friction peak temperature in the ⟨110⟩ direction.

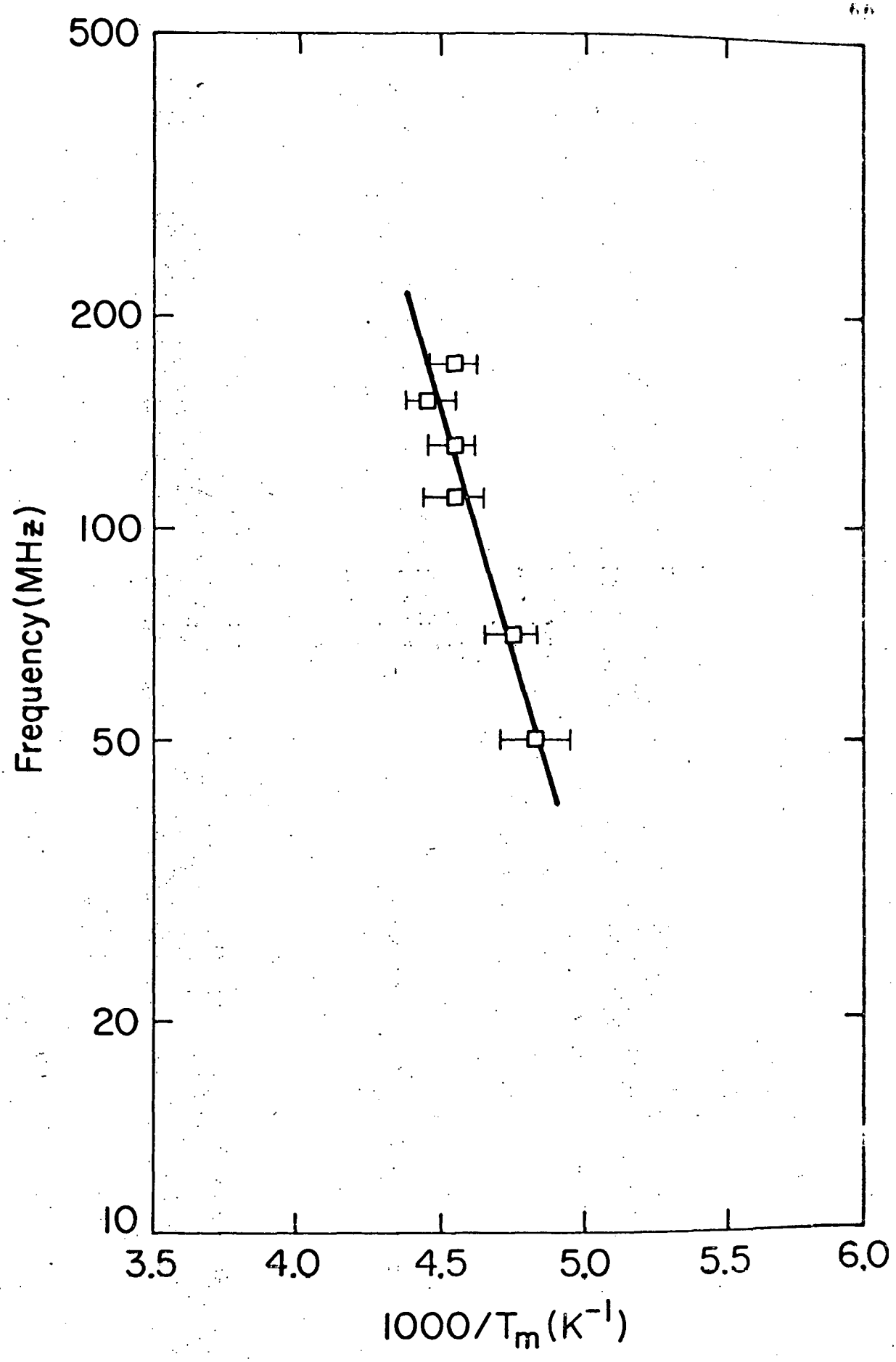
500
200
100
50
20
10
Frequency (MHz)
3.5
4.0
4.5
5.0
5.5
6.0
1000/T_m (K^-1)

Figure 12. The logarithm of the measuring frequency versus the reciprocal of the internal friction peak temperature in the ⟨111⟩ direction.

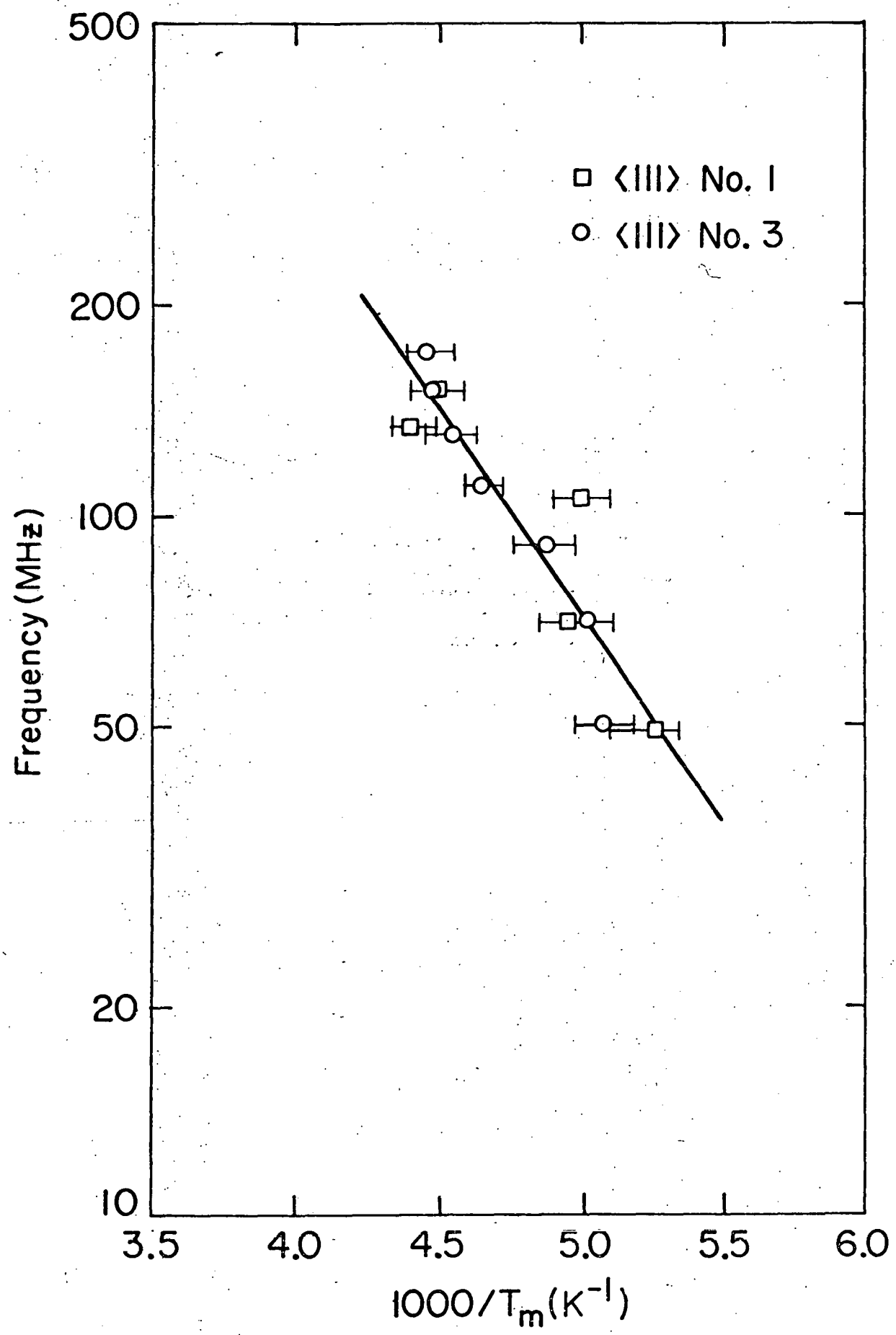
500
200
100
50
20
10
Frequency (MHz)
□ ⟨111⟩ No. 1
○ ⟨111⟩ No. 3
3.5
4.0
4.5
5.0
5.5
6.0
1000/T_m(K^-1)

Table VII

Frequency Factors and Activation Enthalpies

Orientation	ν_o (sec^{-1})	ΔH (eV/atom)
⟨100⟩	1.9×10^{12}	0.18 ± .02
⟨110⟩	2.5×10^{14}	0.27 ± .06
⟨111⟩	6.4×10^{10}	0.12 ± .03

significantly different from each other, and the particular value of ΔH_{100} (along with ν_{o100}) agrees very well with the value found by Mattas and Birnbaum[4] who used the same relaxation mode. The straight lines defined by the parameters of Table VII have been plotted separately in Figures 10 through 12 and together for comparison in Figure 13.

If the internal friction peaks are true Debye peaks with a single relaxation time which obeys Equation (21), then their half-widths in reciprocal temperature can be related to the appropriate activation enthalpy by

$$\Delta(T^{-1}) = T_{-\frac{1}{2}}^{-1} - T_{+\frac{1}{2}}^{-1}$$

$$= \frac{2.634k}{\Delta H} \qquad (31)$$

where $T_{-\frac{1}{2}}$ and $T_{+\frac{1}{2}}$ are the lower and upper temperatures, respectively, that define the half-width. The experimental $\Delta(T^{-1})_{exp}$ and the ratios between these values and the theoretical half-widths, $\Delta(T^{-1})_{th}$, calculated using Equation (31) are shown in Table VI. Experimental difficulties generally preclude ideal half-widths for internal friction peaks, so that somewhat larger measured half-widths are not surprising. As can be seen in Table VI the ratio of experimentally measured half-width to theoretical half-width varies from 1.1 to 1.8 for the ⟨100⟩ and ⟨111⟩ (specimen 3) data, but varies from 1.9 to 2.4 for the ⟨110⟩ propagation direction. The experimental half-widths found in the ⟨110⟩ are actually similar to those found in the

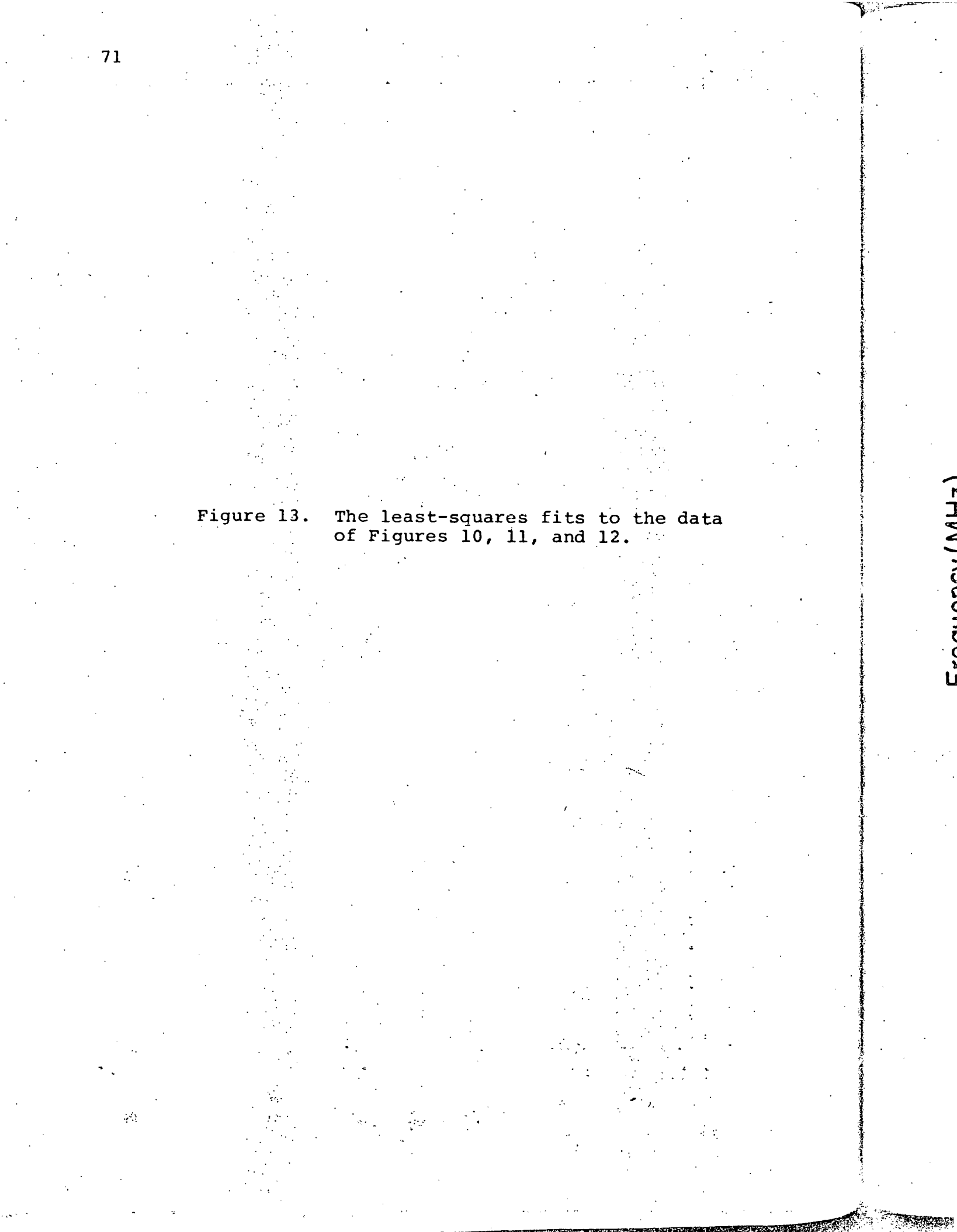

Figure 13. The least-squares fits to the data of Figures 10, 11, and 12.

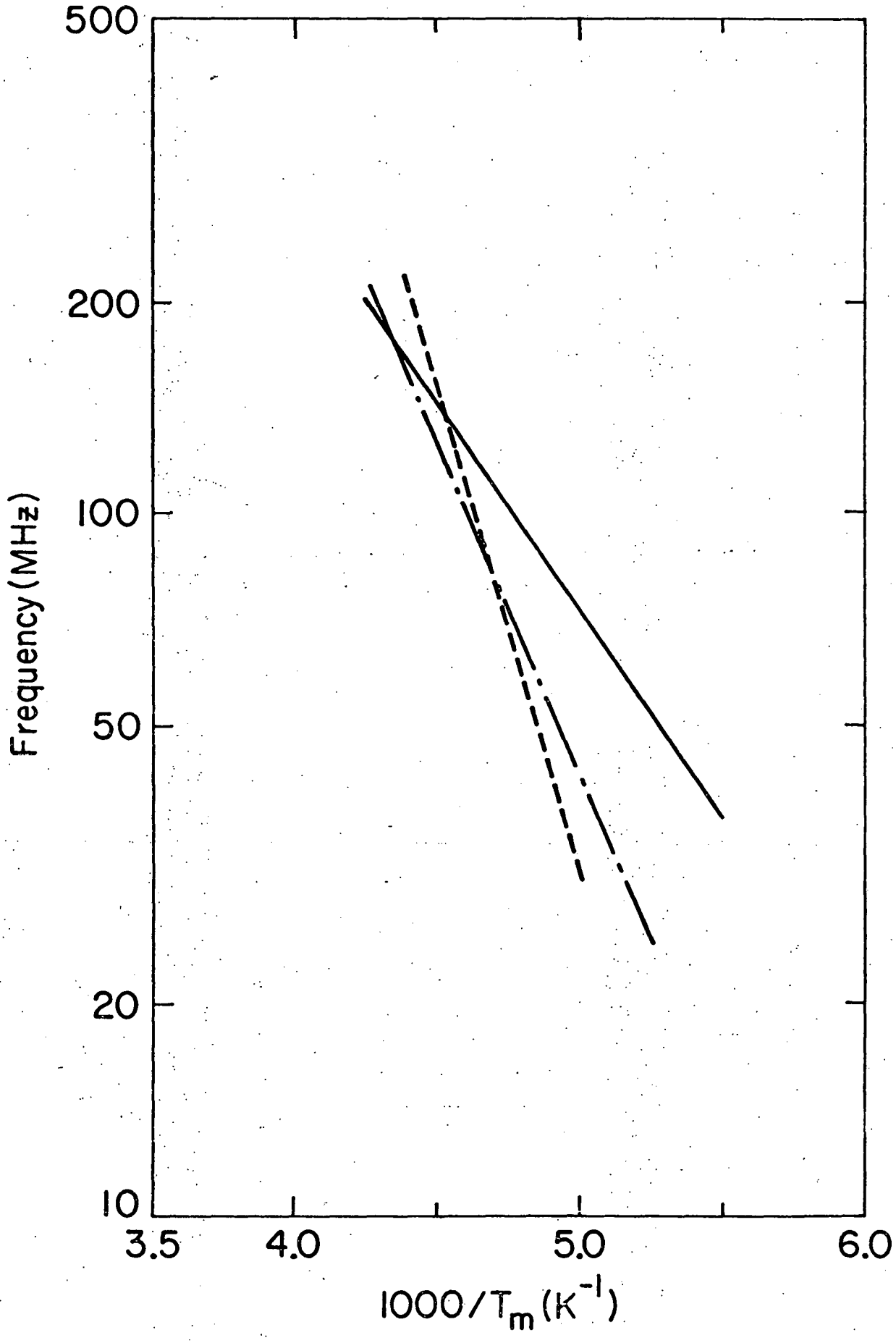
500
200
100
50
20
10
Frequency (MHz)
3.5
4.0
5.0
6.0
1000/T_m (K^-1)

other directions, so that these larger ratios in the ⟨110⟩ direction arise from an anomalously small $\Delta(T^{-1})_{th}$ (i.e., from an anomalously large ΔH_{110}).

The anelastic relaxation strength is inversely proportional to temperature according to Equation (16) and also depends upon temperature indirectly through the concentration of complex defects as shown by Equation (20). Thus the product $T_m Q_m^{-1}$ varies with temperature as the concentration of O-H pairs varies. $T_m Q_m^{-1}$ has been plotted as a function of T_m^{-1} in Figures 14, 15, and 16 for the ⟨100⟩, ⟨110⟩, and ⟨111⟩ (specimen 3) propagation directions, respectively. As a first approximation, the data have been fitted by the method of least-squares to the equation $\log T_m Q_m^{-1} = \log A + B/kT$ where A contains the temperature independent part of the relaxation strength and B is the binding energy. The high temperature limit of the pair concentration (i.e., the form of Equation (17)) has been assumed. The binding energies in the ⟨100⟩ and ⟨111⟩ directions are 0.1 ± .03 and 0.08 ± .02 eV/atom respectively, while a value of 0.2 ± .05 eV/atom was found in the ⟨110⟩ direction. The ⟨100⟩ and ⟨111⟩ results are equal to within the experimental error, and also equal the binding energy deduced by Mattas and Birnbaum.[4]

The assumption of the high temperature limit for pair concentration dependence is seen to be a poor approximation in Figure 17, where the straight lines represent solutions of Equation (17) with C_O and C_H taken as the total solute concentrations, i.e., the high temperature approximation, and where

Figure 14. The logarithm of the product $T_m Q_m^{-1}$ versus reciprocal peak temperature in the ⟨100⟩ direction.

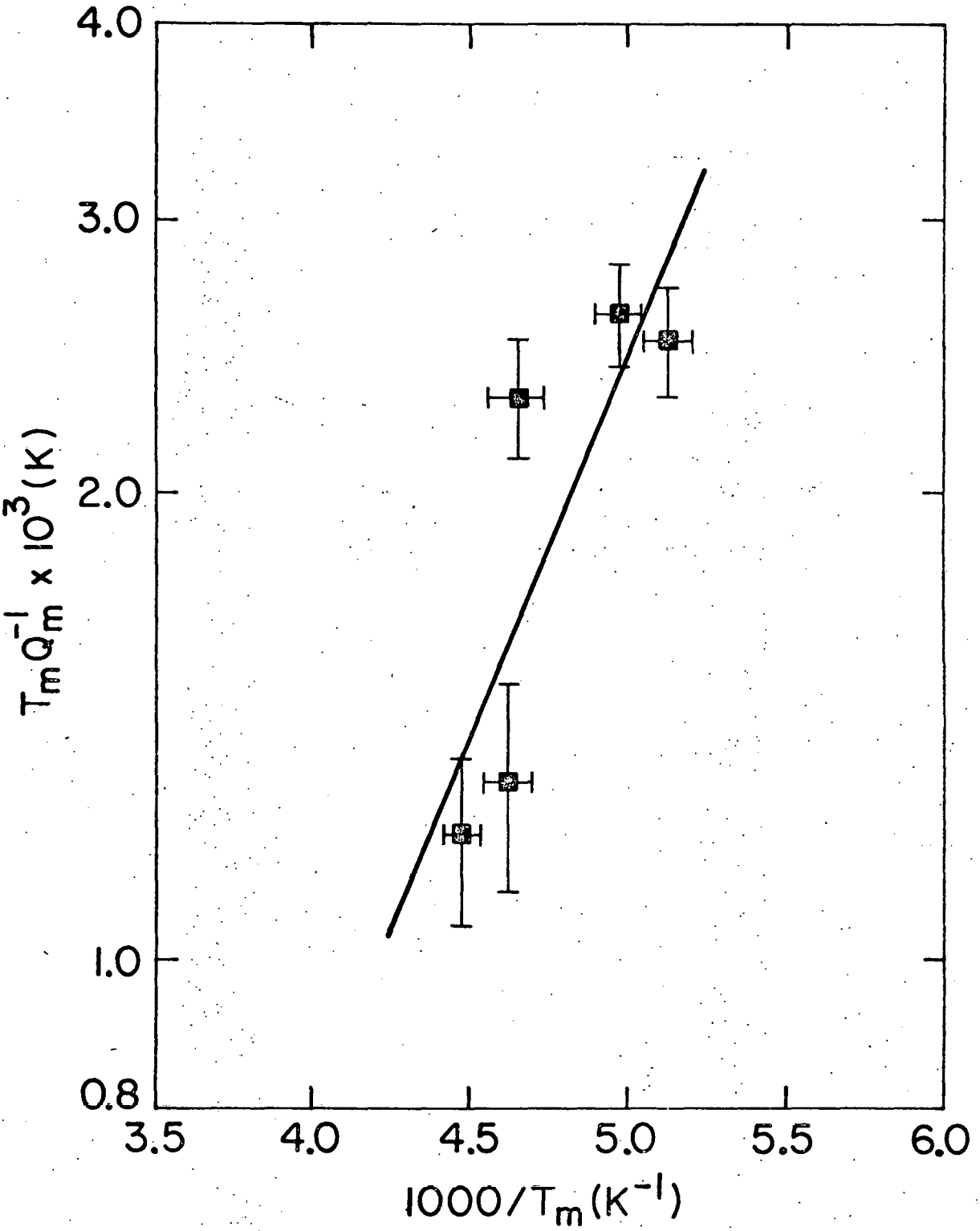
4.0
3.0
2.0
1.0
0.8
3.5
4.0
4.5
5.0
5.5
6.0
$T_m Q_m^{-1} \times 10^3 (K)$
$1000/T_m (K^{-1})$

Figure 15. The logarithm of the product of $T_m Q_m^{-1}$ versus reciprocal peak temperature in the ⟨110⟩ direction.

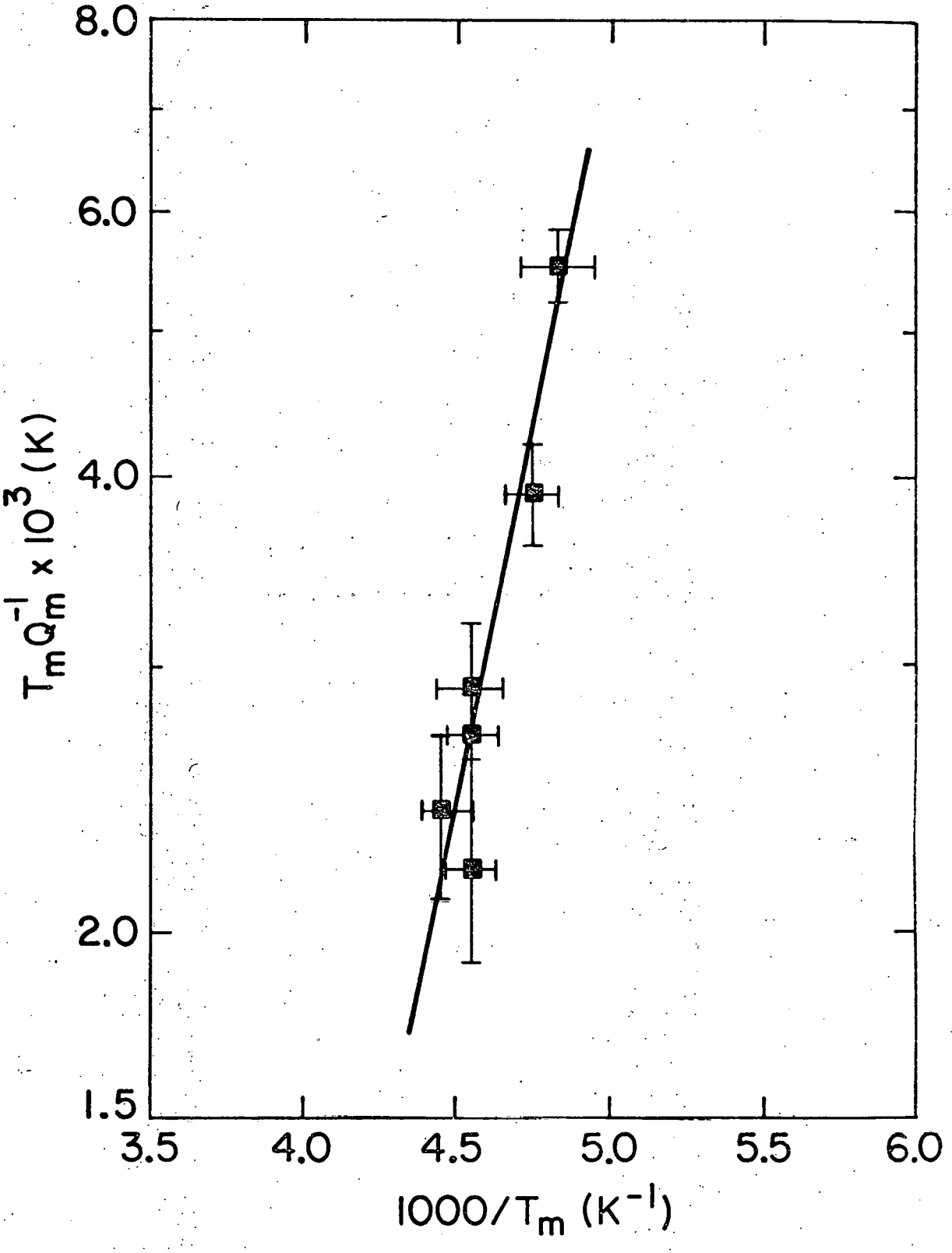
8.0
6.0
4.0
2.0
1.5
$T_m Q_m^{-1} \times 10^3$ (K)
3.5
4.0
4.5
5.0
5.5
6.0
$1000/T_m$ (K^{-1})

Figure 16. The logarithm of the product $T_m\Omega_m^{-1}$ versus reciprocal peak temperature in the ⟨111⟩ direction.

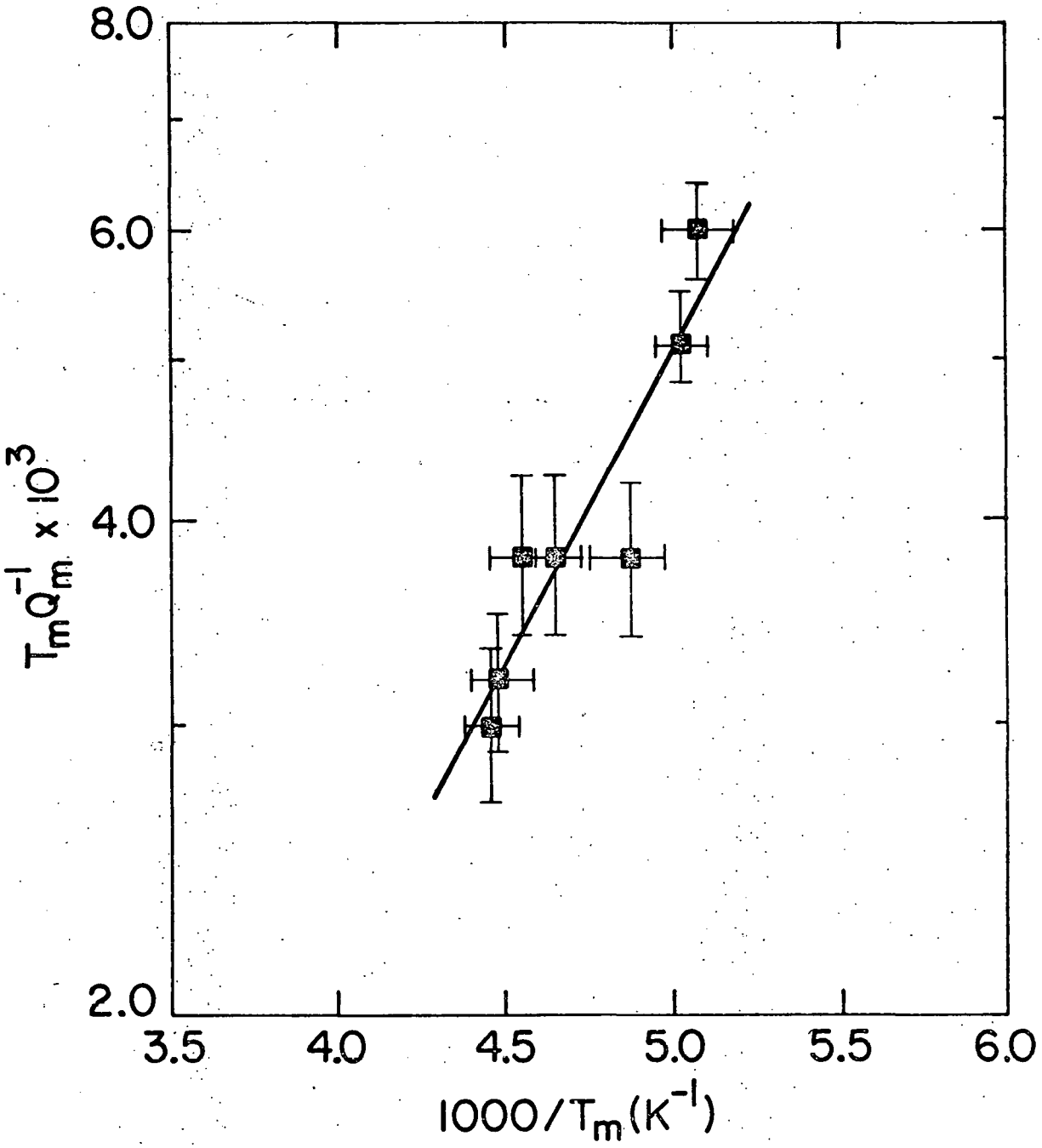
8.0
6.0
4.0
2.0
$T_m Q_m^{-1} \times 10^3$
3.5
4.0
4.5
5.0
5.5
6.0
$1000/T_m(K^{-1})$

Figure 17. The logarithm of the ratio of the concentration of O-H pairs to the total hydrogen concentration versus reciprocal temperature. The numbers indicate the binding energies B in eV/atom. The curved lines represent solutions to Equation (20), and the straight lines represent the high temperature approximation.

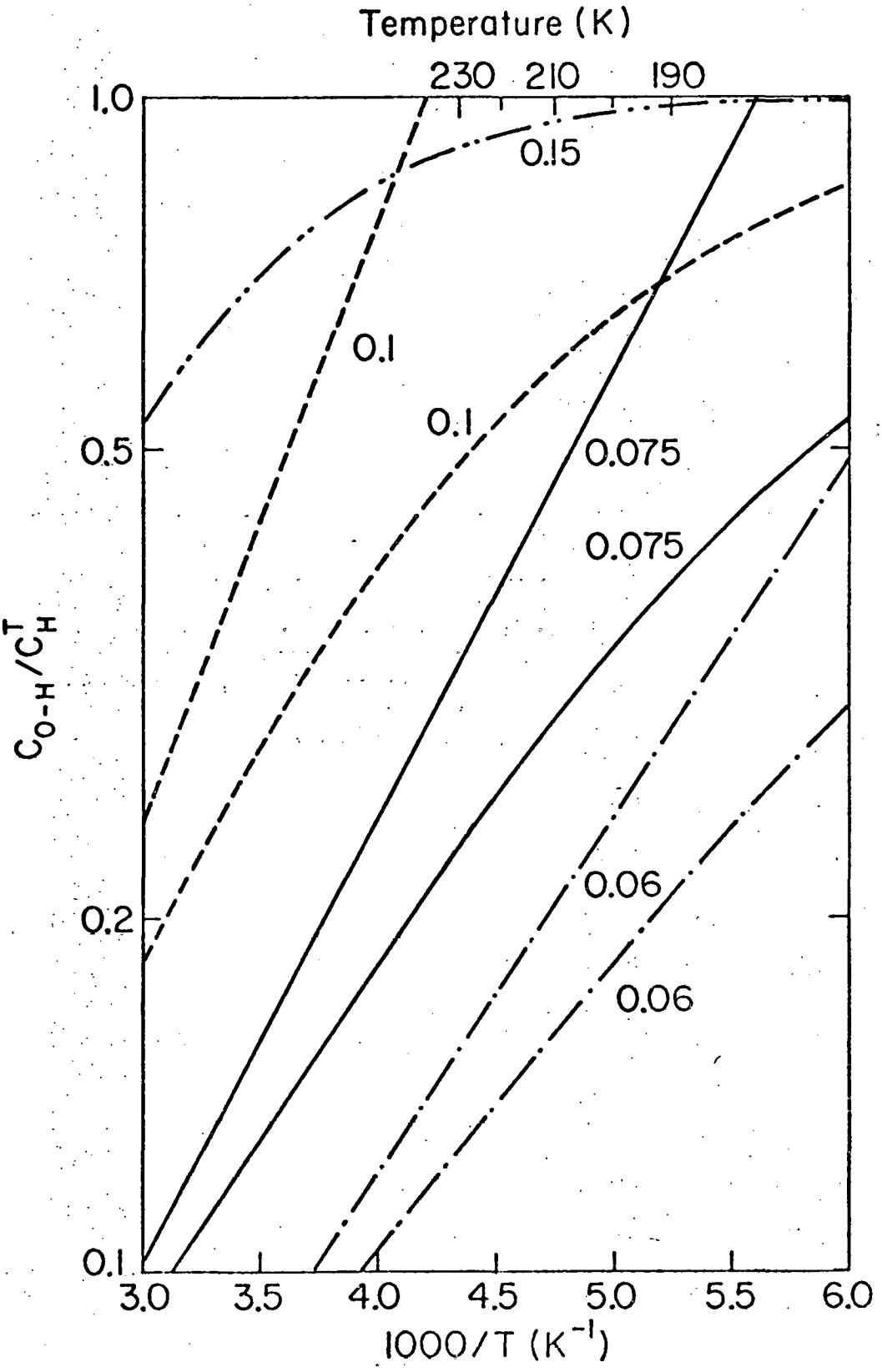
Temperature (K)
230
210
190
1.0
0.5
0.2
0.1
0.15
0.1
0.1
0.075
0.075
0.06
0.06
C_{O-H}/C_H^T
3.0
3.5
4.0
4.5
5.0
5.5
6.0
1000/T (K^{-1})

the curved lines represent solutions of Equation (20), which accounts for solute depletion. The concentration of oxygen-hydrogen pairs has been evaluated using the O and H concentrations of specimen 2 and the values of 3 for the number of interstitial sites per Nb atom, β and 4 for the number of bound sites, z. In the temperature range of the present experiment, 190 to 230K, the depletion of single atoms of the pair constituents results in a considerable reduction of the rate of change of log C_{OH} with reciprocal temperature. In this temperature range the disagreement between the slope of the high temperature limit solution and the tangent of the exact solution of Equation (20) increases as the binding energy increases, since with higher B, C_{OH} approaches the temperature independent limit C_H^T (for $C_H^T < C_O^T$) at higher temperatures. Since B = 0 also produces a temperature independent concentration of pairs equal to that produced by random association of O and H atoms, a value of B exists which maximizes the derivative $d \log(C_{OH}/C_H^T)/dT^{-1}$ at 210K, the center of the experimental temperature range. The derivative is expressed as an apparent binding energy B_{app}, and B_{app} is plotted as a function of B in Figure 18 where it can be seen that B_{app} achieves a maximum value of 0.049 eV/atom at B = 0.069 eV/atom. The maximum in B_{app} depends weakly upon the solute concentrations and somewhat more strongly upon the quotient β/z, with a larger β/z giving a larger B_{app} located at higher B. However the factor β/z is limited to a physically reasonable maximum of 1.5. The slopes

Figure 18. The apparent binding energy B_{app}, taken as the slope of $\log (C_{O-H}/C_H^T)$ at 210K, versus the actual binding energy B. For the solid curve $\beta/z = 0.75$, and for the dashed curve $\beta/z = 1.5$.

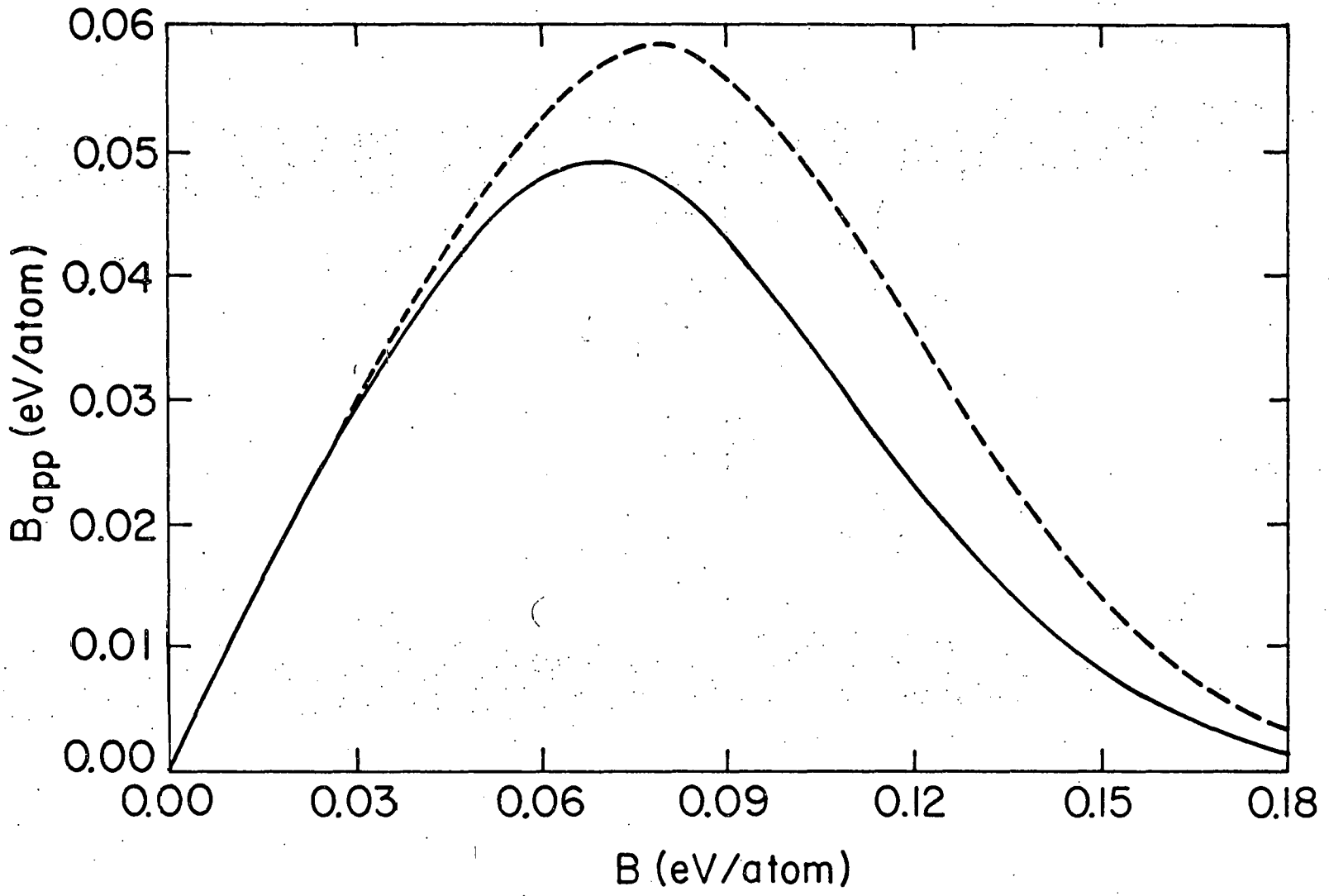
0.06
0.05
0.04
0.03
0.02
0.01
0.00
B_{app} (eV/atom)
0.00
0.03
0.06
0.09
0.12
0.15
0.18
B (eV/atom)

in Figures 14 through 16 are thus clearly in excess of the largest possible B_{app}, for reasons not completely understood. (A value of about 10 for β/z is needed to raise the maximum B_{app} to the values obtained from the slopes in Figures 14 through 16.) A large temperature dependence of Q_m^{-1} may suggest a relaxation strength Δ (Equation (16)) which has the explicit temperature dependence $\Delta \propto (T - T_o)^{-1}$ where T_o is the temperature at which spontaneous ordering of the strain dipoles occurs. T_o measures the strength of the elastic dipole interactions. An attempt to account for the discrepancy between B_{app}^{max} and the experimental values obtained from Figures 14 through 16 by elastic interactions between O-H pairs leads to an interaction energy of 0.05 eV/at.% defects, which results in a spontaneous ordering temperature of about 150K for the O-H concentrations used in the present experiments. This O-H interaction energy may be compared to the value of 0.0021 eV/at.% obtained for H-H interactions in Nb by Gorsky effect measurements.[19] No evidence of spontaneous ordering was seen (Figures 7 through 9) at 150K. Thus, the value of 0.05 eV/at.% which is a factor of 25 larger than that of the H-H interactions, is probably not accurate. The true binding energy of the O-H pairs in niobium is probably of the same order as the 0.12 eV/atom obtained for N-H pairs.[42] At present we can offer no explanation for why the measured values of B (Figures 14 through 16) exceed the theoretical maximum values of B_{app}.

However, for purposes of developing a model of the O-H structure, the significant point is that the apparent binding energies in the ⟨100⟩ and ⟨111⟩ directions are equivalent.

At this point it must be recognized that the relaxation measured in the ⟨110⟩ direction is not independent of those of the ⟨100⟩ and ⟨111⟩ directions. The general tensile compliance J of Equation (11) varies with orientation through the factor Γ. The orientation factor Γ varies from zero when the stress is in a ⟨100⟩ direction to 1/3 in the ⟨111⟩ direction. It can be seen that J_{100} and J_{111} assume quite simple forms in terms of s, s', and s"; with these expressions Equation (11) may be rewritten as

$$J = J_{100} - 3(J_{100} - J_{111})\Gamma . \qquad (32)$$

The compliance in a particular direction must obey the equation $\delta J = J_R - J_U$ in the presence of anelastic relaxation so that, regardless of the underlying mechanism, the relaxation of the compliance must be given by a linear combination of δJ_{100} and δJ_{111}. In particular,

$$\delta J_{110} = \frac{1}{4}\,\delta J_{100} + \frac{3}{4}\,\delta J_{111} . \qquad (33)$$

The experimentally measured quantity is Q_m^{-1} which, from Equation (3) is equal to $\delta J/2J_U$. Thus

$$Q_{m,110}^{-1} J_{U,110} = \frac{1}{4}\,Q_{m,100}^{-1} J_{U,100} + \frac{3}{4}\,Q_{m,111}^{-1} J_{U,111} . \qquad (34)$$

The unrelaxed compliances are calculated from the elastic compliances of niobium: $s_{11} = 0.660 \times 10^{-12}$ cm^2/dyne, $s_{12} = -0.233 \times 10^{-12}$ cm^2/dyne, and $s_{44} = 3.48 \times 10^{-12}$ cm^2/dyne.[59] After substitution of the J_U and division by $J_{U,110}$, Equation (34) becomes

$$Q_{m,110}^{-1} = 0.153Q_{m,100}^{-1} + 0.854Q_{m,111}^{-1} . \qquad (35)$$

As can be seen in Table VI the damping maxima in the ⟨111⟩ direction exceed, at most frequencies, those in the ⟨110⟩ direction, which are in turn larger than those in the ⟨100⟩ direction. The Q_m^{-1} experimental data generally obey Equation (35) quite well. A comparison of the experimental and calculated ⟨110⟩ peak heights is presented in Table VIII.

In view of the agreement shown in this table and in view of the similarity among the damping peak half-widths measured in all three orientations, the large values of ΔH_{110} and B_{110} must be considered somewhat anomalous. The ⟨110⟩ relaxation is necessarily the sum of relaxations measured in the ⟨100⟩ and ⟨111⟩ directions which have relaxation times nearly equal in magnitude but different in their temperature dependence. Thus the temperature dependence of the relaxation time and the product $T_m Q_m^{-1}$ of the ⟨110⟩ relaxation reflects the complex interaction among these relaxations. Since no additional information is obtained from the ⟨110⟩ data (Equation (33)), the analysis of the structure of the O-H defect will be based upon

Table VIII

Comparison of ⟨110⟩ Data with Equation (35)

Frequency (MHz)	Experimental $Q_m^{-1} \times 10^5$	Calculated $Q_m^{-1} \times 10^5$
50	2.6	2.8
70	1.8	2.3
110	1.2	1.6
130	1.3	1.6

the internal friction data measured in the ⟨100⟩ and ⟨111⟩ directions.

Consideration of the structure of the O-H pair must begin with the site occupancy of the solute atoms. The interstitial locations of hydrogen and oxygen in niobium have been identified by neutron scattering and ion channeling experiments. Oxygen atoms have been shown to occupy exclusively the octahedral interstices by Matyash et al.[60] and Carstanjen.[61] Neutron structure analysis and diffuse scattering experiments have demonstrated that hydrogen is largely excluded from the octahedral positions and is distributed between tetrahedral and triangular sites,[35] where the latter site is located at the $0,\frac{3}{8},\frac{3}{8}$ position, midway between nearest neighbor tetrahedral interstices (Figure 19). The occupation probability is appreciably larger in the tetrahedral sites. As was mentioned in Section 2.2, the hydrogen tunnel-state model of Birnbaum and Flynn[28] proposes that hydrogen atoms are not localized on one tetrahedral or triangular site but occupy, at several quantized energy levels, an "orbit" composed of both types of sites probably centered upon an octahedral position. The hydrogen solute is self-trapped in a particular ring by the long-range distortion field of the rapidly tunnelling hydrogen. This model adequately predicts several low temperature properties of hydrogen in niobium including heat capacity[28] and low temperature elastic properties.[27]

Figure 19. (a) The interstitial sites in the b.c.c. lattice: ●, octahedral site; ■, tetrahedral site; and ▲, triangular site.

(b) The ring of tetrahedral and triangular sites centered on an octahedral site.

After Birnbaum and Flynn (28).

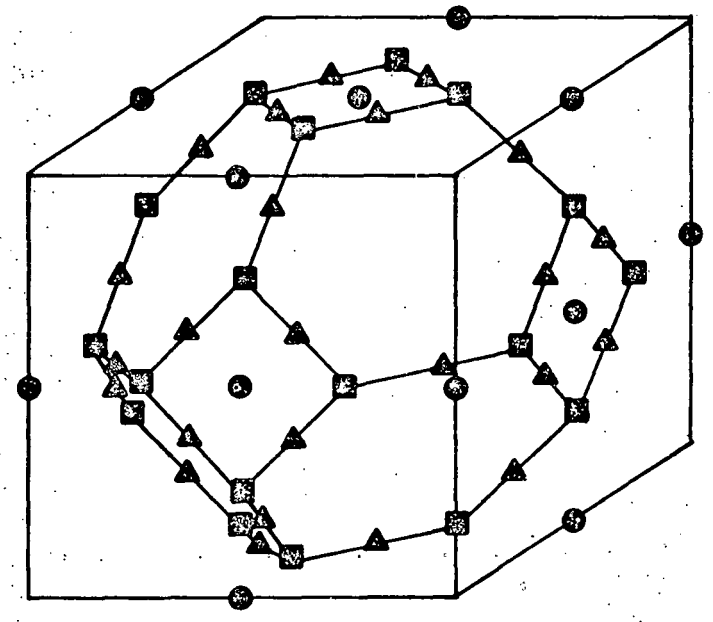

(a)

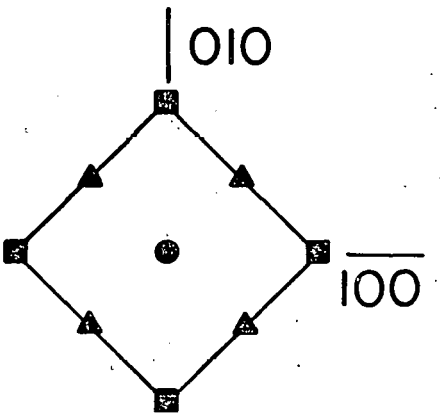

(b)

At the higher temperatures of the present experiment, all the ring energy levels are occupied, and the position of the hydrogen atom may be averaged out to an octahedral site. The transitions among the quantized states occur at about the lattice phonon frequencies which are much greater than the jump frequencies of the anelastic relaxations. The binding of hydrogen to oxygen in the niobium lattice then takes place on the sublattice of octahedral interstices with the assumption that the system of site occupation of individual solutes is applicable to paired atoms. This assumption is supported by the observation that the low temperature properties of the O-H and N-H defects are consistent with the ring occupancy model.[28]

Several attempts have been made to determine the stability and calculate the binding energies of interstitial pairs in b.c.c. metals. The calculations have been based upon elastic interactions between solvent atoms and between solute and solvent atoms. Fisher[62] concluded that stable interstitial carbon pairs form only at the third and fifth nearest neighbor (n.n.) octahedral sites in α-iron, with binding energies of the order of 0.09 eV/atom. Johnson et al.[63] determined that third, fourth, and fifth n.n. carbon pairs in iron should be bound with energies 0.13, 0.11, and 0.08 eV/atom, respectively. The absence of stable closer pairs was attributed to a coulombic repulsion between the carbon atoms. Recently, Blanter and Khachaturyan,[64] using a calculation technique founded on a

lattice statics theory, determined the binding energies of pairs of several kinds of interstitial elements in niobium and other b.c.c. metals. In all cases they calculated first n.n. pairs to be most deeply bound. Application of their calculation techniques to the binding energy of O-H pairs in Nb results in a value of about 0.3 eV/atom for first n.n. pairs and about 0.05 eV/atom for second and third n.n. pairs where octahedral occupancy was used. More distant pairs have lower or negative binding energies. Given the disagreement among theoretical treatments, the development of an O-H pair model will proceed with the consideration of first, second, and third nearest neighbor octahedral pair configurations. The respective point symmetries of these pairs are ⟨100⟩ orthorhombic, ⟨100⟩ monoclinic and ⟨110⟩ monoclinic.

In the consideration of a model of one or more defect symmetries from Table I, it will be assumed that relaxation of the s" hydrostatic compliance is negligible. Although the uniaxial stress applied to the niobium single crystals does produce a hydrostatic response, it is about an order of magnitude smaller than the shear responses. Moreover, s" can relax only if there exist different atomic volumes for the possible symmetries of the defect. While the differences in atomic volume for different O-H pairings are difficult to calculate directly, and have not been measured, it may be noted that no difference in volume of solution between hydrogen and deuterium is measured in niobium,[65] despite the large relative mass

increase. With the neglect of any $\delta s''$, the relaxations of the tensile compliances in the two independent directions are $\delta J_{100} = \delta s'/3$ and $\delta J_{111} = \delta s/3$. Thus under this condition the ⟨100⟩ and ⟨111⟩ data must arise from separate relaxation processes.

The point symmetries identified for the first, second, and third n.n. pairs generate many relaxation times as can be seen in Table III. However, at the low temperatures of the present experiment, the spectrum of relaxation times is modified by the immobility of the oxygen member of the defect pair. Pair reorientation under stress can only occur by hydrogen jumping. Clearly a fixed position for the oxygen atom excludes the possibility of reorientation into some of the crystallographically equivalent sites of the defect. For example, of the six positions of the ⟨100⟩ orthorhombic symmetry pair only two are accessible by hydrogen jumping about a fixed oxygen position. Similarly only four of the twelve orientations of the ⟨100⟩ and ⟨110⟩ monoclinic symmetry pairs are accessible. The immobility of the oxygen atom in effect reduces to zero the reorientation rates into the inaccessible sites. Only at sufficiently high temperatures and low stress frequencies do these rates become significant. (Of course at higher temperatures the O-H pair concentration may be too small to permit the relaxation process to be measured.) Such a division of reorientation rates into high and low temperature regimes is known as the "frozen-free split."[47]

The low temperature reorientation rates are ν_{16} for the ⟨100⟩ orthorhombic symmetry, ν_{12} and ν_{15} for the ⟨100⟩ monoclinic symmetry, and ν_{12} and ν_{17} for the ⟨110⟩ monoclinic symmetry. With the elimination of all other (high temperature) reorientation rates the appropriate relaxation times become those shown below in Table IX. Not only are the expressions for the τ^{-1}'s simplified; there are now fewer of them, as a comparison with Table III will show. This modified spectrum reveals how the phenomenon of the frozen-free split apparently raises the symmetries of the three postulated O-H pairs. The ⟨100⟩ orthorhombic defect has one s' relaxation, like a tetrahedral defect. The ⟨100⟩ monoclinic defect resembles the ⟨110⟩ orthorhombic with one s and one s' relaxation, and the ⟨110⟩ monoclinic defect has lost its s' relaxation so that, like the trigonal symmetry defect, it can not cause a relaxation for a longitudinal wave in the ⟨100⟩ direction.

The principal experimental results to be accounted for by the model are (1) the presence of internal friction peaks in both the ⟨100⟩ and ⟨111⟩ directions, (2) the inequality $\Delta H_{100} > \Delta H_{111}$, (3) the condition $\tau_{100}^{-1} < \tau_{111}^{-1}$ in the temperature range of measurement, and (4) the equivalence in the apparent binding energies measured for the ⟨100⟩ and ⟨111⟩ directions. Point (2) will provide the most rigorous test since the reorientation path which gives the low activation enthalpy in the ⟨111⟩ direction must not be available for the induced motion of hydrogen under the ⟨100⟩ stress. From Table I it

Table IX

Low Temperature Relaxation Times

Symmetry	Compliance	τ^{-1}
⟨100⟩ Orthorhombic	s'	$2\nu_{16}$
⟨100⟩ Monoclinic	s	$2\nu_{12} + 2\nu_{15}$
	s'	$4\nu_{15}$
⟨110⟩ Monoclinic	s	$2\nu_{12} + 2\nu_{17}$ and $4\nu_{12}$

can be seen that several of the defect symmetries can not account for the data by themselves since they do not generate relaxations in both independent directions. Among the closely spaced O-H pairs, the ⟨100⟩ monoclinic symmetry defect and a combination of the ⟨100⟩ orthorhombic and ⟨110⟩ monoclinic symmetry defects satisfy point (1), and models based on these symmetries will be discussed in detail.

The first model considered is based on the presence of second n.n. pairs having ⟨100⟩ monoclinic symmetry. Figure 20(a) illustrates the three crystallographically equivalent orientations of this defect when the oxygen atom is located as shown. It is postulated that first and third n.n. sites are not strongly bound sites with respect to the oxygen atom and so do not contribute to the internal friction. Since all the relaxations result from one defect species, the apparent binding energies in the ⟨100⟩ and ⟨111⟩ directions are necessarily equal as is observed. The hydrogen atom can move around the fixed oxygen atom by first n.n. and second n.n. diffusive jumps, the paths of which are shown in Figure 20(a). The first n.n. jump is characterized by a thermally activated rate, w_1, and the second n.n. jump by rate w_2. Jumps to more distant octahedral sites are considered to be of low probability as they require dissociation of the pair. The reorientation from $H_{(1)}$ to $H_{(2)}$ is seen to occur by two first n.n. jumps (via an intermediate ⟨100⟩ orthorhombic site, designated 'α'), while the

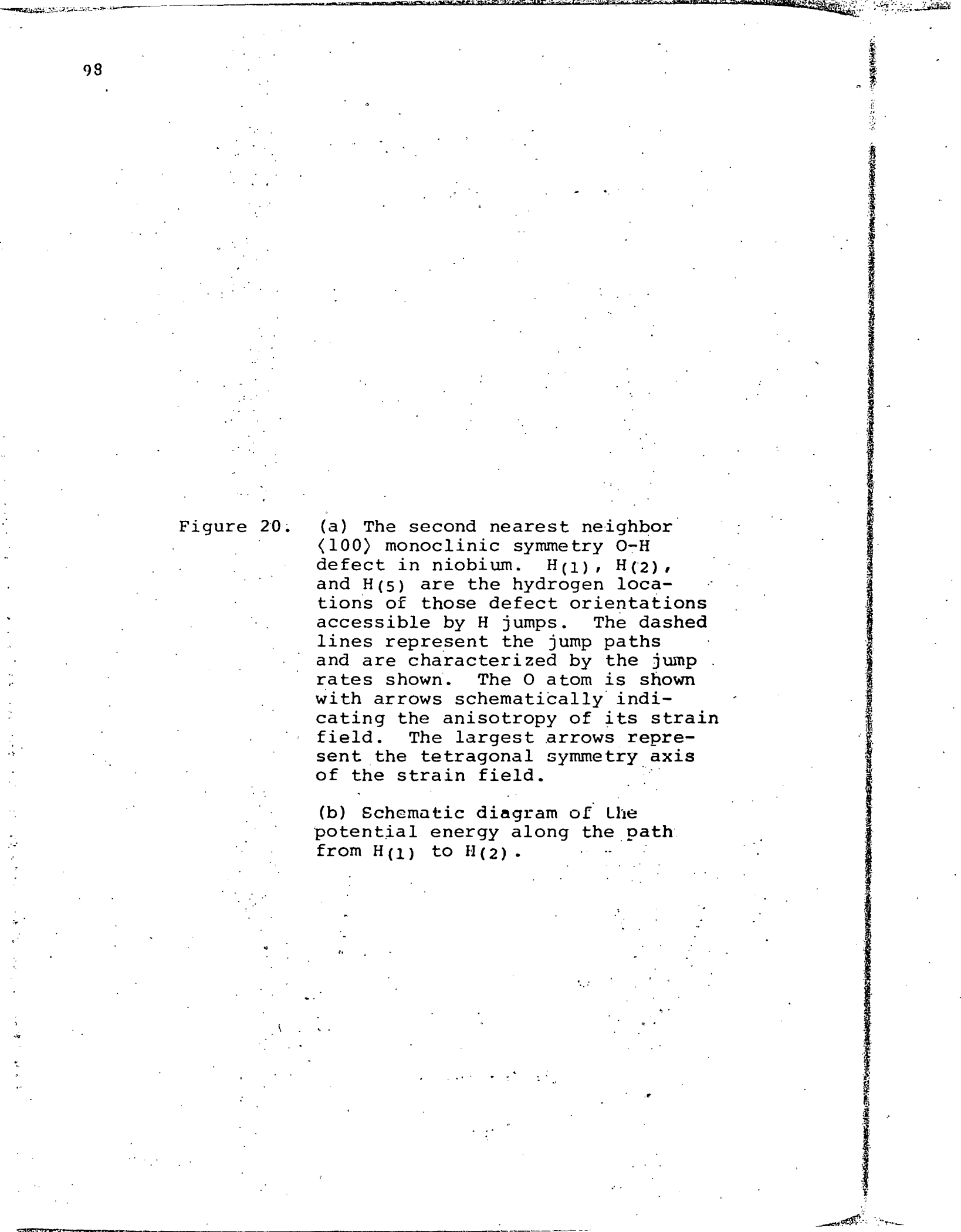

Figure 20. (a) The second nearest neighbor ⟨100⟩ monoclinic symmetry O-H defect in niobium. $H_{(1)}$, $H_{(2)}$, and $H_{(5)}$ are the hydrogen locations of those defect orientations accessible by H jumps. The dashed lines represent the jump paths and are characterized by the jump rates shown. The O atom is shown with arrows schematically indicating the anisotropy of its strain field. The largest arrows represent the tetragonal symmetry axis of the strain field.

(b) Schematic diagram of the potential energy along the path from $H_{(1)}$ to $H_{(2)}$.

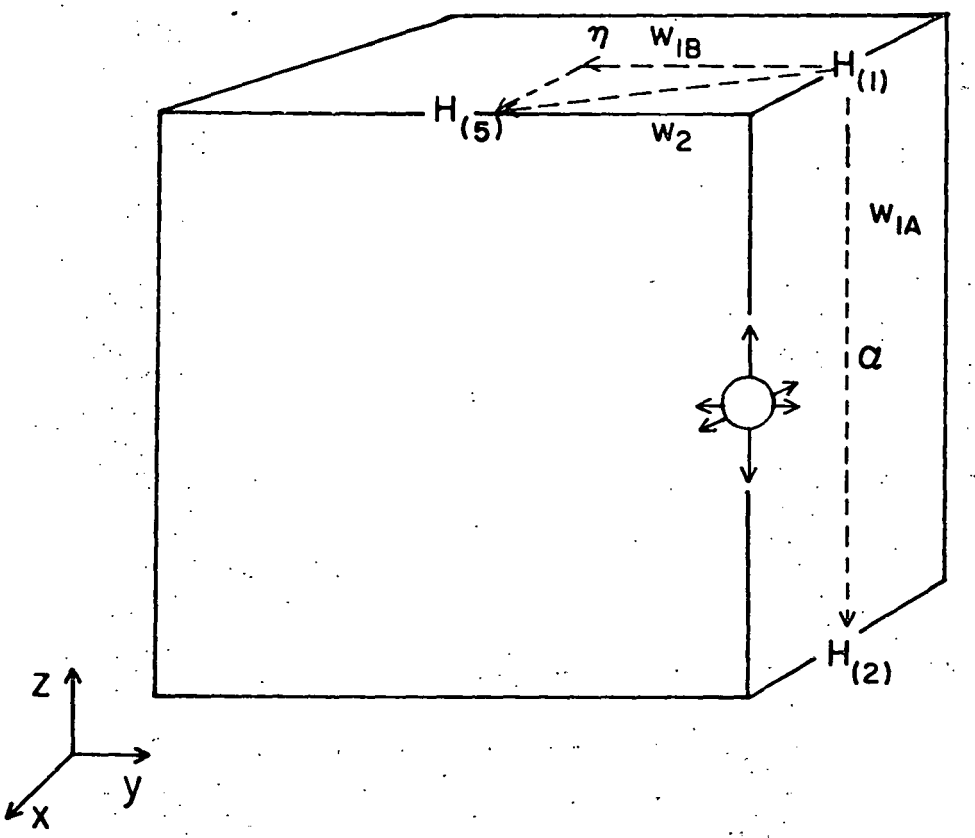

(a)

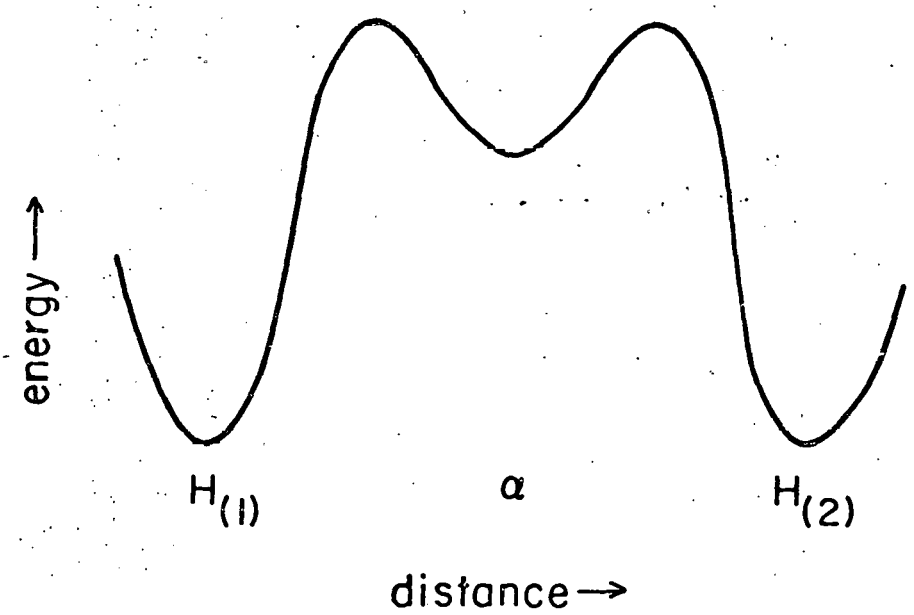

(b)

reorientation from $H_{(1)}$ to $H_{(5)}$ may proceed by two first n.n. jumps (via an intermediate ⟨110⟩ monoclinic or 'η' site) or one second n.n. jump.

Since the ⟨100⟩ monoclinic symmetry sites are more deeply bound than the α or η sites in this model, different activation barriers will obtain for jumps into and out of the various sites. The potential energy of the hydrogen atom as a function of distance is shown schematically for the $H_{(1)}$ to $H_{(2)}$ reorientation in Figure 20(b). The effective jump frequency from $H_{(1)}$ to $H_{(2)}$ may be obtained by analogy with the one-dimensional motion of dimers on solid surfaces.[66] In the latter system the dimer is considered to have two differently configured bound states with different binding energies. The diffusion of the center of mass of the dimer is characterized by two jump rates a and b, where a is the jump rate from the strongly bound to the weakly bound configuration and b is the rate of the reverse jump. Over long times the mean square displacement of a single dimer's center of mass is characterized by an effective jump frequency given by $ab/(a + b)$. For a large population of hydrogen atoms which reorient by two first n.n. jumps, a jump frequency similar to that given above obtains. Because of the exponential dependence of the jump frequencies on the respective activation enthalpies, ΔH_a and ΔH_b, the value of $ab/(a + b)$ is within 1% of a in the temperature range of interest for ratios of $\Delta H_a/\Delta H_b > 2$. This inequality is consistent with the postulated weak O-H binding for hydrogen occupation of α or η

sites. Hence the reorientation by two first n.n. jumps can be characterized by one jump frequency w_1 and one activation enthalpy ΔH_1.

While w_1 is degenerate among the ⟨100⟩ jump directions in a cubic symmetry lattice, in the present experiment this degeneracy is lifted by the local tetragonal symmetry strain provided by the oxygen interstitial. The principal values of the oxygen dipole moment tensor are $P_1 = 11.8$ eV and $P_2 = P_3 = 4.9$ eV;[67] P_i is related to the strain tensor component λ_i by $P_i = (3/2)(\Omega/K)\lambda_i$, where Ω is the atomic volume and K is the compressibility. Thus, rather different strains are encountered in the jumps of hydrogen parallel and perpendicular to the tetragonal axis of the oxygen strain field, and this will result in different activation enthalpies for the two types of jumps. In Fig. 20(a) the tetragonal axis of the oxygen atom is oriented in a vertical direction (i.e., in the direction of the nearest neighbor solvent atoms). The reorientation path $H_{(1)}$ to $H_{(2)}$ is parallel to this axis, and the path $H_{(1)}$ to $H_{(5)}$ is perpendicular to it. If the first n.n. jump along the former path is designated w_{1A} and along the latter w_{1B}, the reorientation times may be written (Table IX) $\tau_{100}^{-1} = 4w_{1B} + 4w_2$ and $\tau_{111}^{-1} = 2w_{1A} + 2w_{1B} + 2w_2$. The results $\tau_{100}^{-1} < \tau_{111}^{-1}$ and $\Delta H_{100} > \Delta H_{111}$ require that $w_{1A} > w_{1B}$, $w_{1A} > w_2$ and that w_{1A} have the lowest activation energy (ΔH_{1A}) and dominate the reorientation in the ⟨111⟩ direction, i.e., $\Delta H_{1A} < \Delta H_{1B}$ and $\Delta H_{1A} < \Delta H_2$. Thus within these

restraints on the relevant frequencies and enthalpies, the model based upon a ⟨100⟩ monoclinic O-H pair can account for the observations.

The experimental observations can also be accounted for by a combination of ⟨100⟩ orthorhombic and ⟨110⟩ monoclinic symmetry defects. In this model the second n.n. defect (designated 'β'), i.e., the ⟨100⟩ monoclinic symmetry, is weakly bound. From the previous symmetry discussions it is seen that the ⟨100⟩ relaxation is due to the ⟨100⟩ orthorhombic pair and the relaxation in the ⟨111⟩ direction is due to the ⟨110⟩ monoclinic pair. The two defects are postulated to have equal O-H binding enthalpies in accordance with point (3) above. Figures 21(a) and 22 show the atomic arrangements and reorientation paths of the accessible sites of the ⟨100⟩ orthorhombic and ⟨110⟩ monoclinic O-H pairs, respectively. A schematic potential energy diagram for the reorientation of the ⟨100⟩ orthorhombic defect via first n.n. jumps is shown in Figure 21(b). There are two weakly bound β sites and one strongly bound η site along the path from $H_{(1)}$ to $H_{(6)}$. Again the jumps out of the weakly bound sites are very rapid and hence not rate-controlling, so that the significant transitions are from $H_{(1)}$ to $\beta_{(1)}$ and η to $\beta_{(2)}$. These two jumps are asymmetric with respect to the oxygen elastic dipole; the former is parallel to the tetragonal axis of the dipole and is characterized by frequency w_{1A}, while the latter is perpendicular and is characterized by w_{1B}. Two second n.n. reorientation paths

Figure 21. (a) The first nearest neighbor ⟨100⟩ orthorhombic symmetry O-H defect in niobium. $H_{(1)}$ and $H_{(6)}$ are the hydrogen locations of those defect orientations accessible by H jumps, along with rates w_{1A}, w_{1B}, w_2, w_2'. The O atom is shown with arrows indicating the anisotropy of its strain field.

(b) Schematic diagram of the potential energy along the path from $H_{(1)}$ to $H_{(6)}$.

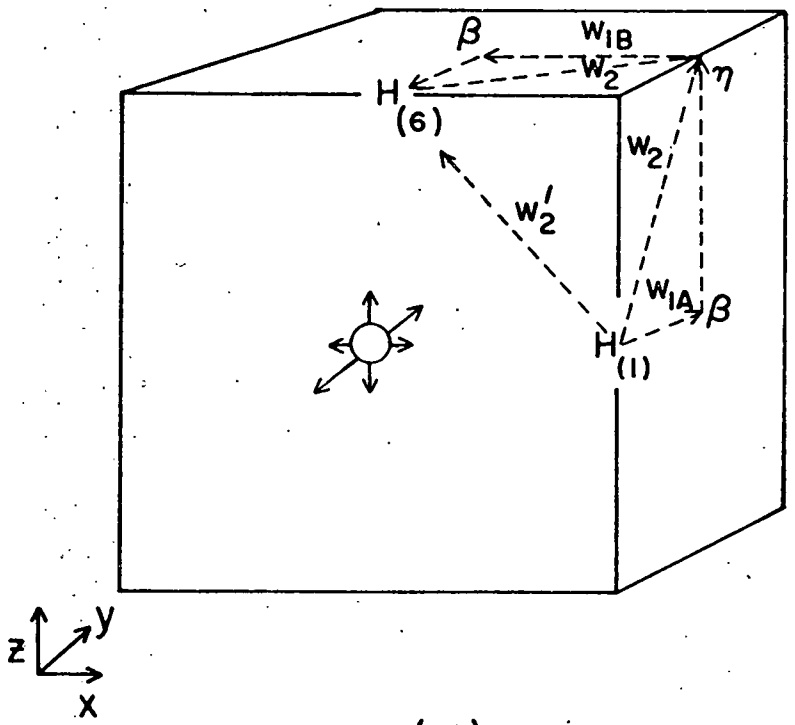

(a)

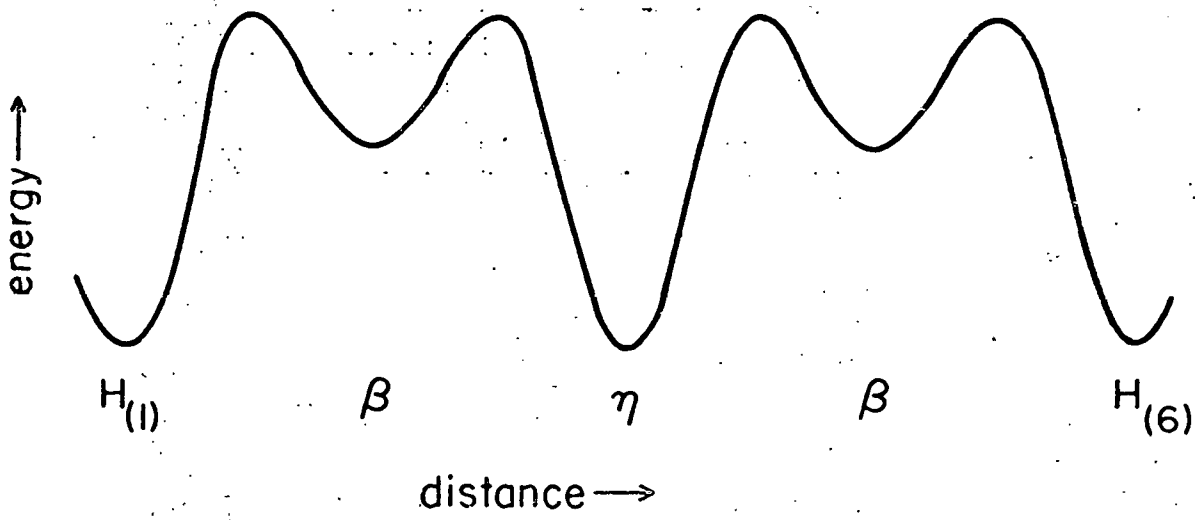

(b)

Figure 22. The third nearest neighbor ⟨110⟩ monoclinic symmetry O-H defect in niobium. $H_{(1)}$, $H_{(2)}$, and $H_{(7)}$ are the hydrogen positions of those defect orientations accessible by H jumps. The dashed lines indicate the jump paths and are characterized by the rates shown. The O atom is shown with arrows indicating the anisotropy of its strain field.

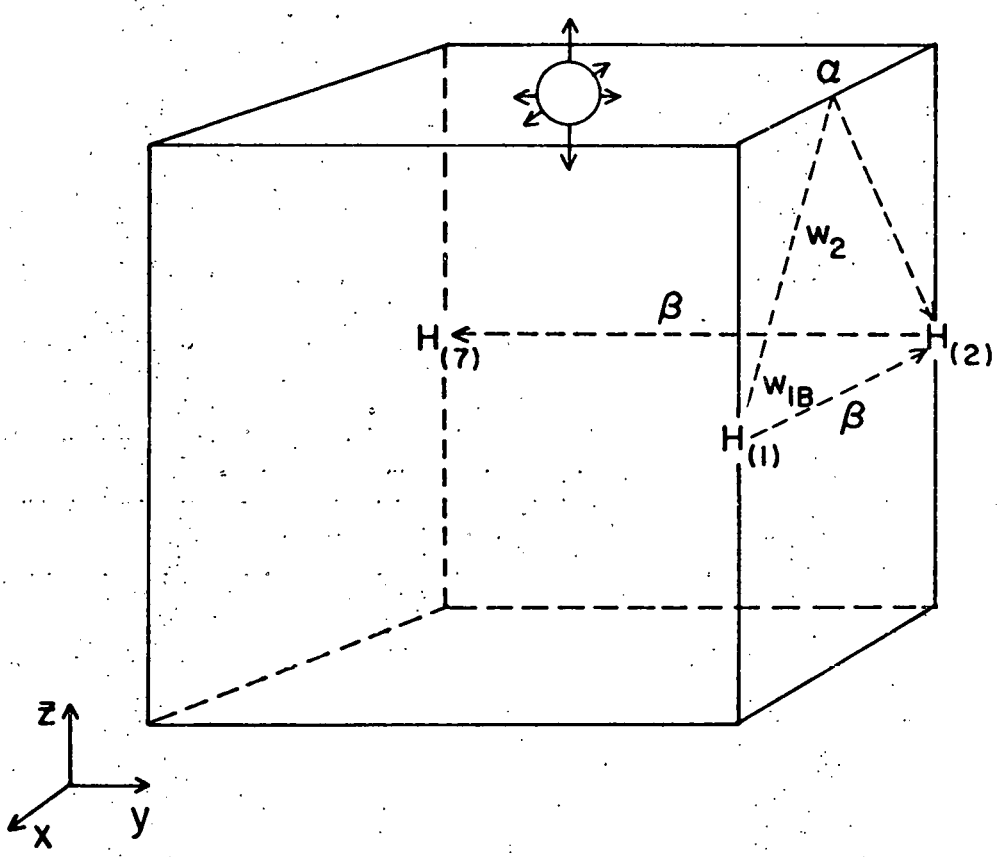
α
w2
β
H(7)
H(2)
wIB
β
H(1)
z
x
y

between $H_{(1)}$ and $H_{(6)}$ are also shown in Figure 21(a). One consists of two jumps each at frequency w_2 and proceeds via the intermediate η position, and the other is a presumably higher energy path, straddled by the oxygen atom and a nearest neighbor niobium atom, with a jump frequency w_2' different from w_2. Thus the reciprocal relaxation time τ_{100}^{-1} due to the reorientation of the ⟨100⟩ orthorhombic defect is

$$\tau_{100}^{-1} = 8 \frac{w_{1A}w_{1B}}{w_{1A} + w_{1B}} + 8w_2 + 4w_2'.$$

The ⟨110⟩ monoclinic symmetry defect generates two ⟨111⟩ relaxations, which are characterized by $\tau_{111,1}^{-1} = 2\nu_{12} + 2\nu_{17}$ and $\tau_{111,2}^{-1} = 4\nu_{12}$. As shown in Figure 22 the defect may reorient under stress from its $H_{(1)}$ to $H_{(2)}$ position by two first n.n. jumps via an intermediate β site or by two second n.n. jumps via an intermediate α site. The path of the first n.n. jump lies perpendicular to the oxygen tetragonal strain axis, and so the frequency w_{1B} applies. The second n.n. jump is again described by frequency w_2. The same types of jump also apply to the reorientation from $H_{(1)}$ to $H_{(7)}$. Since the temperature dependence of the relaxation time (i.e., the activation enthalpy) is the parameter of interest, only one relaxation time need be presented viz. $\tau_{111}^{-1} = 4w_{1B} + 4w_2$.

The experimental results can be explained with this two-defect model if w_{1B} is the highest hydrogen jump frequency and $\Delta H_{1B} < \Delta H_{1A}$. It should be observed that in the expression for

τ_{100}^{-1} for the relaxation of the ⟨100⟩ orthorhombic defect, the term $8(w_{1A}w_{1B}/w_{1A} + w_{1B})$ tends to $8w_{1A}$ when $w_{1B} > w_{1A}$. Thus $\tau_{111}^{-1} > \tau_{100}^{-1}$ and $\Delta H_{111} < \Delta H_{100}$.

Of course the dominant jump frequency can not be predicted for the ⟨100⟩ orthorhombic defect, even with this highly simplified model. It is significant however that the condition $w_{1B} > w_{1A}$ required for the two-defect model to satisfy the experimental results is the inverse of the condition required for the ⟨110⟩ orthorhombic defect to satisfy them. The two models are thus mutually exclusive. The results in fact can not be explained with the defect symmetries discussed if there is no difference between w_{1A} and w_{1B}.

Another possibility which should be considered is that all three O-H pairs are present. In this case the ⟨100⟩ orthorhombic pair (nearest neighbor) contributes to a relaxation measured in the ⟨100⟩ direction with a relaxation frequency

$$\tau_{100}^{-1(1n)} = 8\,\frac{w_{1A}w_{1B}}{w_{1A} + w_{1B}} + 8w_2 + 4w_2'$$

and the ⟨100⟩ monoclinic pair (second nearest neighbor) contributes a relaxation with a frequency

$$\tau_{100}^{-1(2n)} = 4w_{1B} + 4w_2 .$$

The total relaxation observed in the ⟨100⟩ direction is described by the sum of the two relaxations. Similarly in the ⟨111⟩ direction the total relaxation is the sum of that due to the

⟨100⟩ monoclinic pair and that due to the ⟨110⟩ monoclinic (third nearest neighbor) pair.

$$\tau_{111}^{-1(2n)} = 2w_{1A} + 2w_{1B} + 2w_2$$

$$\tau_{111}^{-1(3n)} = 4w_{1B} + 4w_2 \ .$$

In this model the three pairs are required to have approximately equal binding enthalpies. The observation that $\Delta H_{100} > \Delta H_{111}$ can now be considered using the above four expressions. In order to simplify the considerations the jump frequencies w_2 and w_2' will be taken as small compared to the first nearest neighbor jump frequencies. The assumption $w_{1B} > w_{1A}$ and $\Delta H_{1B} < \Delta H_{1A}$ leads to

$$\tau_{100}^{-1(1n)} = 8w_{1A}$$

$$\tau_{100}^{-1(2n)} = 4w_{1B}$$

$$\tau_{111}^{-1(2n)} = 2w_{1B}$$

$$\tau_{111}^{-1(3n)} = 4w_{1B} \ .$$

Both the ⟨100⟩ and ⟨111⟩ relaxations are the sum of two Debye relaxations with the ⟨111⟩ having a width of twice the ideal width and the ⟨100⟩ having a width which increases as the temperature is decreased.

If we assume $w_{1A} > w_{1B}$ and $\Delta H_{1A} < \Delta H_{1B}$ the relaxation frequencies are

$$\tau_{100}^{-1(1n)} = 8w_{1B}$$

$$\tau_{100}^{-1(2n)} = 4w_{1B}$$

$$\tau_{111}^{-1(2n)} = 2w_{1A}$$

$$\tau_{111}^{-1(3n)} = 4w_{1B} .$$

Again both relaxation modes have greater than the ideal width with the ⟨100⟩ data having a width of twice the ideal and ⟨111⟩ having a temperature dependent width.

As seen from the above discussion, the data do not allow a definitive selection among the possible mechanisms. The conditions under which each of the models can satisfy the experimental observations are given in Table X. It may be noted that the model in which all three types of pairs are present results in multiple relaxations for the ⟨100⟩ and ⟨111⟩ longitudinal modes. In this case one of the modes should have a temperature independent width of about twice that of a single Debye relaxation and the other mode should have a width which increases as the temperature decreases. As shown in Table VI the ⟨100⟩ and ⟨111⟩ widths are almost equal to the ideal Debye width at the higher temperatures and both increase as the temperature decreases. The damping peaks are small and the data have relatively large errors due to difficulties in establishing the background damping. Thus while the data suggest that the model with all three O-H pairs present is not appropriate, it can not be definitely discarded.

Table X

Conditions for Model Applicability

Pairs	Conditions Required	Conclusions
⟨100⟩ Monoclinic 2nd nearest neighbor	$B_{\langle 100\rangle mono} > B_{\langle 100\rangle ortho}$	(a) 2nd nearest neighbor pairs are stable
	$B_{\langle 100\rangle mono} > B_{\langle 110\rangle mono}$	(b) $B_{100} = B_{111} = B_{OH}$
	$w_{1A} > w_{1B}$	(c) $\tau_{100}^{-1} = 4w_{1B}$
	$w_{1A} >> w_2$	$\tau_{111}^{-1} = 2w_{1A} + 2w_{1B}$
⟨100⟩ Orthorhombic 1st nearest neighbor	$B_{\langle 100\rangle ortho} = B_{\langle 110\rangle mono}$	(a) 1st and 3rd nearest neighbor pairs are stable
	$B_{\langle 100\rangle ortho} > B_{\langle 100\rangle mono}$	(b) $B_{100} = B_{111}$
⟨110⟩ Monoclinic 3rd nearest neighbor	$w_{1B} > w_{1A}$	(c) $\tau_{100}^{-1} \simeq 8w_{1A}$
	$w_{1B} >> w_2$	$\tau_{111}^{-1} = 4w_{1B}$

Table X continued

Pairs	Conditions Required	Conclusions
⟨100⟩ Orthorhombic 1st nearest neighbor	$B_{\langle 100\rangle ortho} \simeq B_{\langle 100\rangle mono}$	(a) 1st, 2nd, and 3rd nearest neighbor pairs are stable
	$B_{\langle 100\rangle ortho} \simeq B_{\langle 110\rangle mono}$	
⟨100⟩ Monoclinic 2nd nearest neighbor		(b) $B_{100} = B_{111}$
	$w_{1B} > w_{1A}$	(c) $\tau_{100}^{-1} = 8w_{1A}$
⟨110⟩ Monoclinic 3rd nearest neighbor		$\tau_{100}^{-1} = 4w_{1B}$
		$\tau_{111}^{-1} = 2w_{1B}$
		$\tau_{111}^{-1} = 4w_{1B}$
	or	
	$w_{1A} > w_{1B}$	(c′) $\tau_{100}^{-1} = 8w_{1B}$
		$\tau_{100}^{-1} = 4w_{1B}$
		$\tau_{111}^{-1} = 2w_{1A}$
		$\tau_{111}^{-1} = 4w_{1B}$

As stated previously, more distant pairs than third nearest neighbors have been neglected because they have been assumed not bound. Since the strain field of interstitials falls off as $1/r^3$,[59] there are also kinetic reasons for ignoring the more distant pairs. For, in the analysis above, the anisotropy of the oxygen atom strain field has been assumed to cause the different activation enthalpies measured in the ⟨100⟩ and ⟨111⟩ directions. However at greater pair separations the effect of the anisotropy will be weaker and thus less able to account for the different activation enthalpies.

5.2 Internal Friction and Strain Relaxation in the Nb-N-H System

Internal friction peaks and strain relaxation curves due to hydrogen reorientation around nitrogen solutes were observed in niobium polycrystalline specimens. (The specimens had a ⟨110⟩{110} texture from rolling and had the tension/compression axis parallel to the ⟨110⟩.) Hydrogen-free Nb-N specimens showed no damping peaks and no anelastic strain relaxation. All but two of the internal friction peaks were measured with the constant amplitude method with the specimen driven at its resonance frequency. A typical curve of drive voltage versus temperature for this method is shown in Figure 23. Conversion of drive voltage to the damping parameter Q^{-1} is made with the equation

Figure 23. Resonance frequency and internal friction versus temperature.

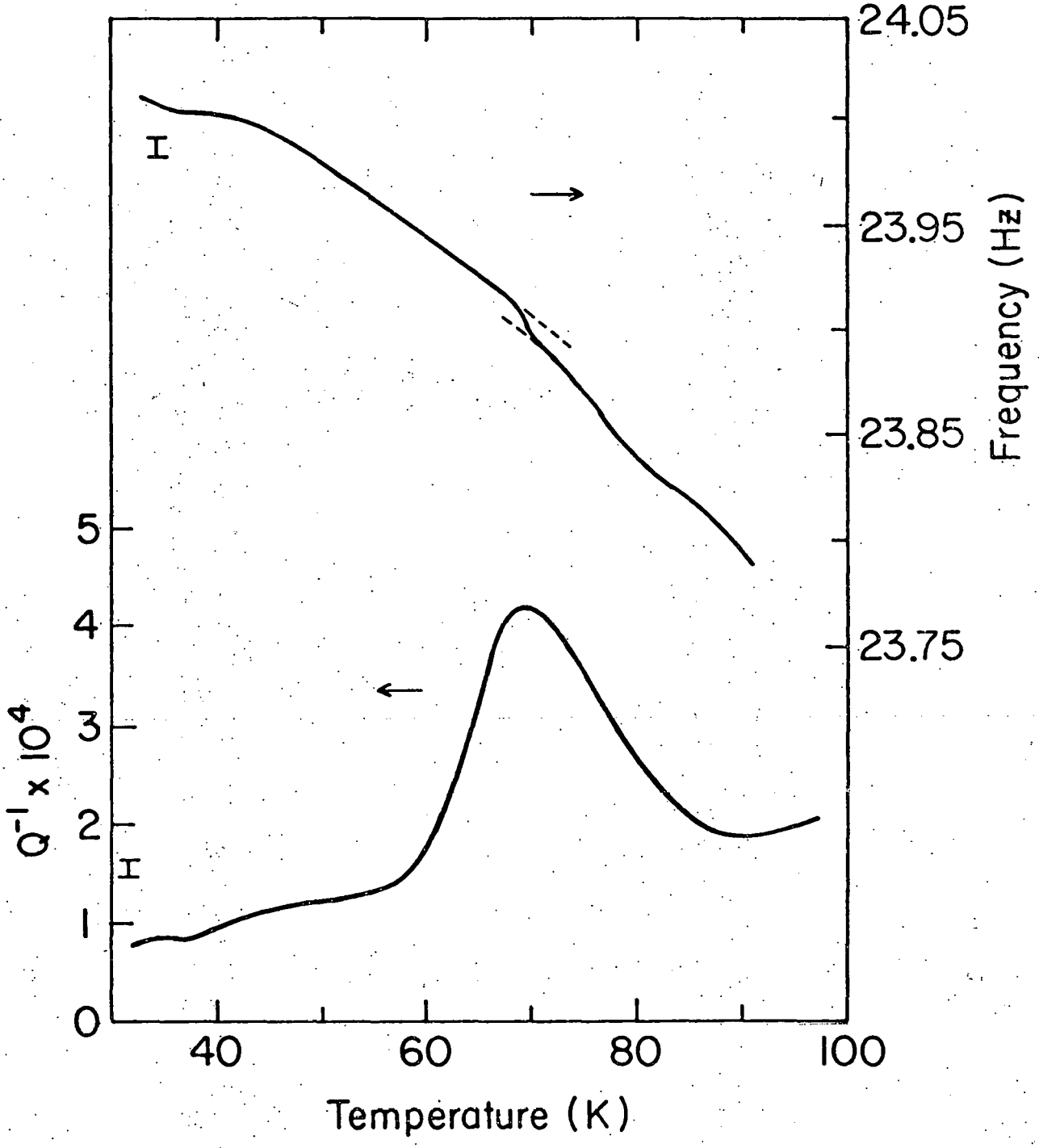
24.05
23.95
23.85
23.75
Frequency (Hz)
I
→
←
H
$Q^{-1} \times 10^4$
0
1
2
3
4
5
40
60
80
100
Temperature (K)

$$Q^{-1} = K \frac{V_{dr}}{V_{pu}}$$

where V_{dr} and V_{pu} are the rms drive and pick-up voltages, respectively, and K is a constant.[68] This constant is determined by direct measurement of the number of vibrations, N, of the specimen in free decay between two amplitudes (i.e., pick-up voltages) v_1 and v_2. V_{dr} and V_{pu} are also measured at the same temperature. Q^{-1} is related to N by

$$Q^{-1} = \frac{1}{\pi N} \ln \frac{v_1}{v_2}$$

where $v_1 > v_2$. The data at 8.4 Hz were obtained with a constant drive voltage at resonance frequency, so that the relaxation was seen as an amplitude minimum. The 3.6 Hz internal friction peak was measured directly with the free decay technique.

The condition for the peak maximum is $\omega_r \tau = 1$, where ω_r is the resonance frequency. In the case of the driven specimens this frequency was taken to be the output frequency of the phase-locked oscillator. The resonance frequency was recorded as a function of temperature so that frequency at maximum damping could be defined (Figure 23). Measurement of ω_r also allowed observation of the small modulus defect, due to hydrogen reorientation since $\omega_r \propto J_1^{-1}$. Experimental error obscured the modulus defect in some runs, but when detectable, it corroborated the temperature of the internal friction maximum. The temperatures of the peak maxima were determined after subtraction of the

slightly temperature-dependent background damping. Measured temperatures were calibrated for the difference in temperature, under vacuum conditions, between the specimen grip and the center of the specimen. The Au-Fe versus chromel thermocouple was calibrated at liquid helium temperature, and the ice-point reference device (Omega Engineering Model TRC) was calibrated against an H_2O triple-point cell. The peak temperatures, resonance frequencies, and peak heights measured in the Nb-N-H system are presented in Table XI.

The product $T_m Q_m^{-1}$ is not systematically temperature dependent in the temperature range of this experiment and had values of 1.8×10^{-2} to 3.6×10^{-2} K. Temperature independence of this quantity is consistent with the behavior predicted by the trapping model discussed in the previous section. With a binding energy of 0.12 eV/atom for the N-H pair (which is the likely configuration for this cluster[42]), nearly complete depletion, of whichever element of the pair is in lower concentration, occurs at the temperatures of this experiment leading to a constant N-H pair concentration.

Hydrogen jump frequencies two orders of magnitude lower than obtained by the internal friction method were measured with the strain relaxation technique. A typical curve of strain as a function of time, representing the anelastic response of specimen 7, is shown in Figure 24. The temperature of the grip was calibrated again to that of the center of the specimen, since He exchange gas at one torr was present in the experimental

Table XI

N-H Internal Friction Data

Peak Temperature (K)	Resonance Frequency (Hz)	Peak Height $Q_m^{-1} \times 10^4$	Specimen
81.2	124.0	4.0	7
80.5	164.0	3.2	7
77.3	93.05	3.9	5
76.8	64.3	4.0	7
73.3	44.11	4.0	5
73.5	32.4	5.0	7
70.5	23.90	2.6	5
69.0	13.5	3.5	5
68.5	9.4	3.2	5
68.0	8.5	3.1	5
67.0	5.21	1.8	5
66.0	3.6	2.0	5

Figure 24. Strain (in units of μV representing the output of the capacitance bridge) versus time.

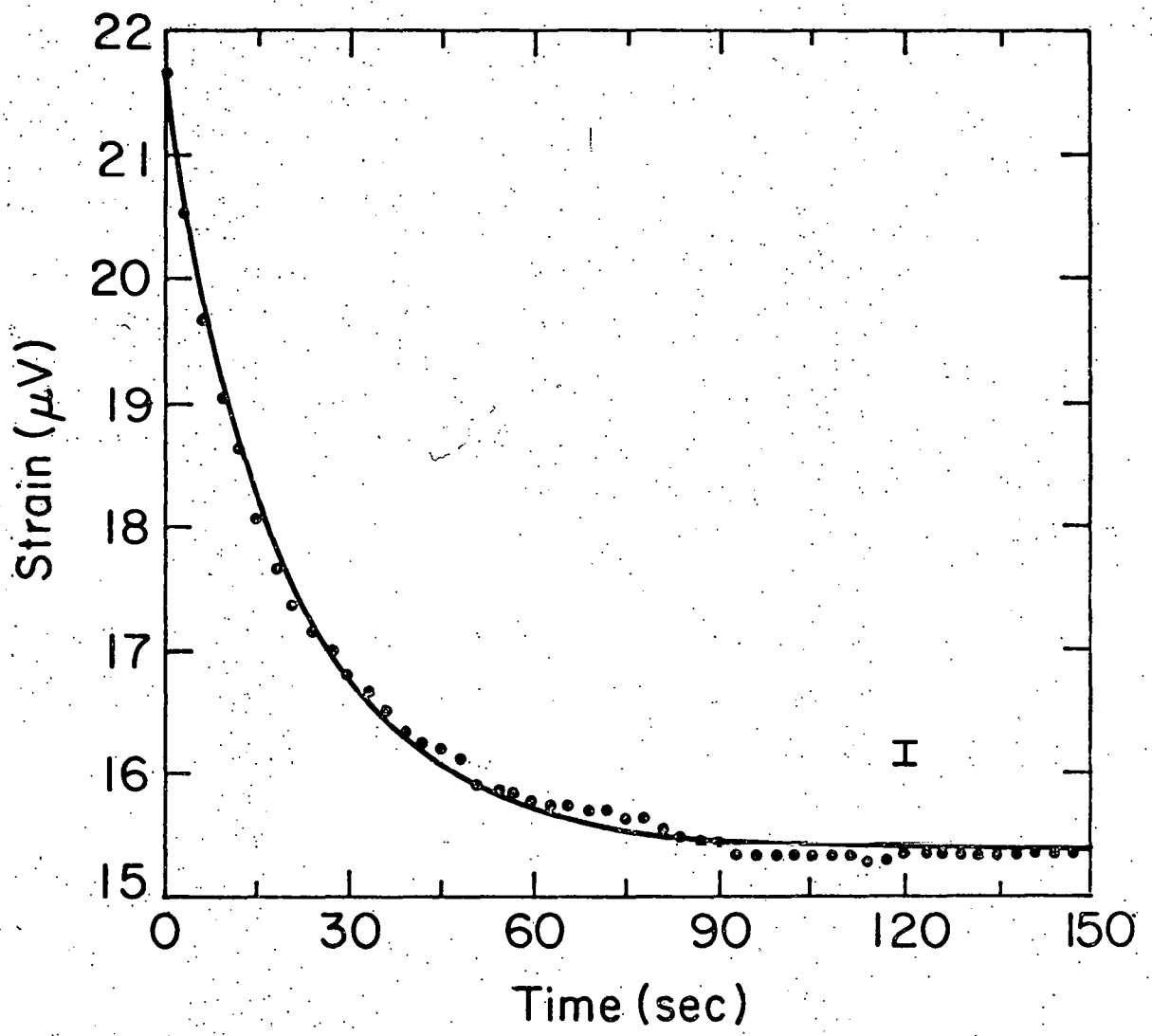
22
21
20
19
18
17
16
15
Strain (μV)
0
30
60
90
120
150
Time (sec)
I

chamber during these measurements. (The gas had no discernible effect on the relaxation times.) The temperature range over which strain relaxation was measured, 39.2 to 57.5K, was determined by the capability of the electronics to record the short relaxation times ($\sim$ 10 sec.) and by the maintenance of temperature stability during measurements over long times. In none of the runs could a stress-induced ordering of hydrogen be quenched in since the equilibrium capacitance (i.e., the capacitance of the undeflected specimen) varied too much with temperature. Rather, the specimen was deflected at the temperature of interest, and the anelastic response allowed to build up for a length of time estimated to equal several relaxation times. Evaporation of the liquid He around the specimen chamber proved to limit the length of time for deflection and measurement. The temperature stability during all runs was sufficient to ensure a time-independent background capacitance.

Each strain relaxation curve was fitted to exponential decay curves of the form $\sum_i A_i \exp(-t/\tau_i) + A(\infty)$. The amplitudes A_i, relaxation times τ_i, and background amplitude (or amplitude at infinite time) were adjusted to provide the best least-squares fit. The quality of the fit was assessed by an iterative calculation of χ^2 for each set of adjustable parameters. The principal component of the computer program was the subroutine "CURFIT" written by Bevington,[69] which is designed to fit experimental data to functions that are non-linear in their coefficients. The algorithm of CURFIT combines

a search for the minimum of χ^2 along the gradient of χ^2 with respect to the adjustable parameters with an analytic solution for the minimization of χ^2 through a linear approximation of the fitting function. The former procedure provides good convergence far from the minimum, while the latter procedure provides rapid convergence near the minimum. The data were fitted to one-, two-, and three-exponential relaxation processes. In the calculations of χ^2 the data were weighted by their normalized amplitudes above background. Fits to three processes generally were redundant with respect to two processes or were unphysical with negative amplitudes or relaxation times. Satisfactory fits were obtained with both one and two relaxation processes. However, in the latter fit the typical ratio of τ_2/τ_1 was between 3 and 4 and such ratios of two relaxation times are not large enough to be considered physically significant within the limits of the fitting procedure. Moreover, in the N-H internal friction measurements only one peak (relaxation process) was seen at each frequency and its width was consistent with a single relaxation. Consequently it may be concluded that the strain relaxation curves are caused by a single relaxation process. The relaxation times, τ, determined in the single process fits are listed in Table XII. The error in temperature measurement is $\pm$ 0.25K, while the error in the relaxation times is estimated to be $\pm$ 20%.

The jump frequencies of nitrogen-trapped hydrogen, (where the frequency $f = 1/2\pi\tau$) are plotted as a function of reciprocal temperature in Figure 25. For comparison the frequencies of

Table XII

N-H Strain Relaxation Data

Temperature (K)	Relaxation Time (sec)
57.5	9.4
56.2	8.9
55.3	10.6
54.5	16.9
54.0	20.6
53.2	17.7
51.6	38.4
50.8	33.2
48.2	68.5
45.4	93.7
43.7	190.4
42.3	442.2
41.5	406.8
39.2	870.2

Figure 25. The logarithm of the hydrogen jump frequency versus reciprocal temperature. O, O-H data, Ref. (2); and ●, N-H data, present work. The solid and dashed curves are calculated from the Flynn-Stoneham theory.

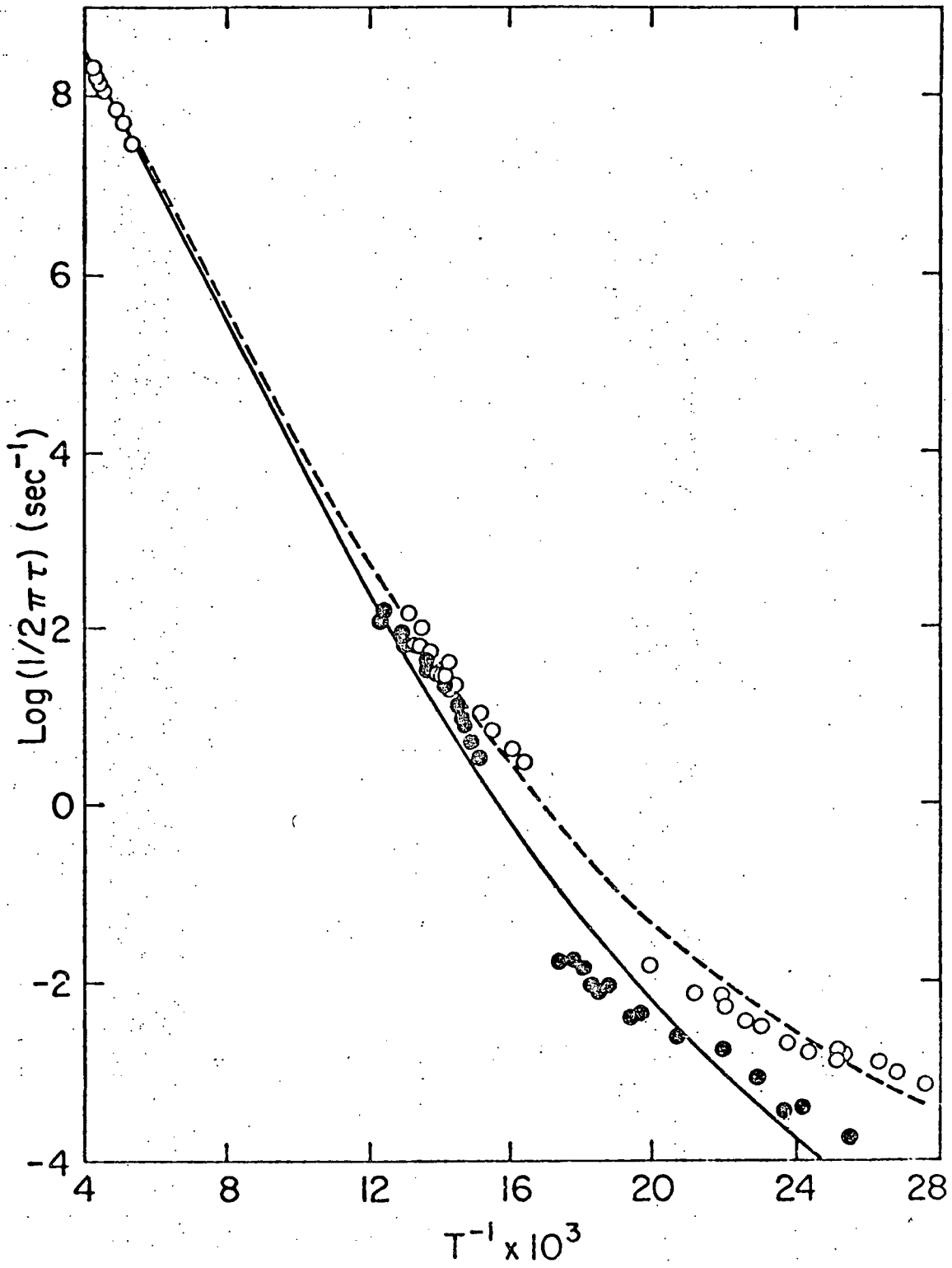
8
6
4
2
0
-2
-4
Log (1/2πτ) (sec⁻¹)
4
8
12
16
20
24
28
T⁻¹ x 10³

oxygen-trapped hydrogen[2] are also shown. As discussed in Section 2.2, these data have been analyzed in terms of the phonon-assisted tunnelling theory of Flynn and Stoneham.[22] Since the N-H data can not be explained by classical diffusion theory (in the form of a single Arrhenius relaxation), these data have also been analyzed in terms of the tunnelling theory.

A least-squares fit of the logarithms of the measured jump frequencies to the logarithms of the hydrogen hopping rate given by Equation (26) was determined with the subroutine CURFIT. The adjustable parameters of the fitting function were the lattice activation energy, E_a, the Debye temperature, θ_D, and the transition matrix element $|J|$. The integrals appearing in Equations (27) and (28) were evaluated by means of a 10-point Gaussian quadrature formula, and a 10-point Gaussian-Hermite quadrature formula was used to evaluate the integral in Equation (26). The computer program employing CURFIT did not converge to a solution when applied to the N-H data. It was determined that this resulted from the absence of high temperature, high frequency data for the N-H relaxation. In order to provide what is in effect a boundary condition to be met by the three adjustable parameters, the jump frequencies measured by Mattas and Birnbaum (and shown in Figure 1) for the O-H reorientation[4] at high temperatures were added to the N-H data. While there are no high temperature N-H reorientation data, the O-H and N-H jump frequencies are comparable above 65K as shown in Figure 25, and diverge below 60K. Thus a good approximation of

the N-H behavior by the high temperature O-H data is expected. With the addition of the O-H data the program converged to the solution depicted by the solid line in Figure 25. All data points were weighted equally in this fitting procedure.

The solid line in Figure 25 was generated by Equation (26) with these values of the adjustable parameters: E_a = 0.222 eV, θ_D = 243.5K, and $|J|$ = 0.239 eV. The O-H data shown in Figure 25 along with the data of Mattas and Birnbaum have been reanalyzed in the manner applied to the N-H data (which differs from the procedure of Chen and Birnbaum in treating $|J|$ as an adjustable parameter over the whole range of data). The results for oxygen-trapped hydrogen reorientation were E_a = 0.207 eV, θ_D = 257.4K, and $|J|$ = 0.111 eV, and the dashed line shows the fit of the O-H data.

While a physical explanation of the absolute values of both sets of parameters is difficult to establish, certain qualitative observations concerning the relative difference between oxygen-trapped and nitrogen-trapped behavior can now be made. The two sets of parameters differ primarily in the value of the transition matrix element $|J|$, with lesser differences in the lattice activation energy and Debye temperature. From Equation (22), $|J|$ or J_{pp}, can be viewed as the extent of the overlap of the hydrogen wave function in the initial state with the wave function in the final state of the transition. Thus a larger physical separation of the initial interstitial site from the final site should produce a lower J_{pp}, which suggests a greater

hydrogen wave function overlap between the p and p' states near the N traps than near the O traps. However, it has not been possible to calculate definitively the displacement of the interstitial sites resulting from nearby oxygen or nitrogen solutes due to a lack of experimental data. There is not even experimental agreement on the volumes of solution of oxygen and nitrogen in niobium.[70-72]

The result that $|J|^{N-H} > |J|^{O-H}$ indicates under the interpretation above that the potential energy barrier between the initial and final sites of the hydrogen atom is narrower in the case of oxygen-trapping. It can be shown that a quantum mechanical particle that tunnels through a potential barrier separating two identical wells does so at a frequency which decreases exponentially with increasing barrier width.[73] Hydrogen trapped by nitrogen thus should jump with a frequency larger than that of oxygen -trapped hydrogen. However, it can be seen in Figure 25 that the jump frequency of oxygen-trapped hydrogen exceeds that of nitrogen-trapped hydrogen at temperatures below 60K. This probably occurs because of the exponential dependence of the jump frequency upon E_a as shown in Equation (24). Comparison of the fitted parameters shows that $E_a^{N-H} > E_a^{O-H}$. The Debye temperatures, which are about equal for the two defect species, represent the local phonon distribution around the interstitial impurities. The influence of these impurities is not large, as θ_D for pure niobium is 275K, obtained by heat capacity measurements.[23]

6. SUMMARY AND CONCLUSIONS

The local motion of hydrogen bound to oxygen and nitrogen solutes in niobium has been studied with anelastic relaxation techniques. Internal friction peaks were measured by ultrasonic attenuation in the ⟨100⟩, ⟨110⟩, and ⟨111⟩ directions of Nb-O-H single crystals using longitudinal mode stress waves. Damping peaks due to O-H pair reorientation were characterized by activation enthalpies of motion of 0.18 eV/atom and 0.12 eV/atom in the ⟨100⟩ and ⟨111⟩ directions, respectively. The jump frequency in the ⟨111⟩ direction exceeded that in the ⟨100⟩ direction over the temperature range of this experiment. However, equal binding energies of about 0.1 eV were measured in the two directions.

The selection rules for anelastic relaxation were applied to establish two likely models for the structure of the O-H defect, under the assumption of octahedral interstitial occupancy for both O and H. The first model consists of a hydrogen atom bound at the second nearest neighbor interstitial site with respect to the oxygen atom. The point symmetry of this pair is ⟨100⟩ monoclinic, and this defect gives rise to both the ⟨100⟩ and ⟨111⟩ relaxations. The second model consists of a first nearest neighbor pair with ⟨100⟩ orthorhombic symmetry, which causes the ⟨100⟩ relaxation, and a third nearest neighbor pair with ⟨110⟩ monoclinic symmetry, which causes the ⟨111⟩ relaxation. A third possible, though less likely, model

involves the presence and reorientation of all three of the above-mentioned pairs. It was inferred that the difference between the ⟨100⟩ and ⟨111⟩ activation enthalpies is due to the motion, during reorientation, of the hydrogen atom along different paths within the tetragonal symmetry strain field of the oxygen atom. However a specific choice from among the three models can not be made based on anelastic relaxation data.

In Nb-N-H polycrystalline specimens the jump frequency of hydrogen below 100K was measured with low frequency internal friction and strain relaxation methods. The jump frequency of hydrogen trapped at nitrogen solutes was found to deviate markedly from a classical Arrhenius temperature dependence below about 50K. The data were analyzed in terms of the Flynn-Stoneham theory of the phonon-assisted tunnelling of light interstitials. By comparison with the jump frequency of oxygen-trapped hydrogen, the nitrogen-trapped hydrogen data were displaced toward lower frequencies. This displacement was reflected in changes in the parameters of the Flynn-Stoneham theory, the most significant change occurring in the transition matrix element $J_{pp'}$, between the initial and final hydrogen states. The N-H matrix element is more than twice the O-H matrix element, and the lattice activation enthalpy determined from the N-H data is larger than that determined from the O-H data. The values of these parameters as well as those of the Debye temperatures are physically reasonable, and it is concluded that the N-H data, in addition to the O-H data, are in good agreement with the Flynn-Stoneham theory.

REFERENCES

1. J. Völkl and G. Alefeld, Diffusion in Solids: Recent Developments, edited by A. S. Nowick and J. J. Burton, p. 272, Academic Press, New York (1975).

2. C. G. Chen and H. K. Birnbaum, Phys. Stat. Sol. (a) 36, 687 (1976).

3. C. C. Baker and H. K. Birnbaum, Acta Met. 21, 865 (1973).

4. R. F. Mattas and H. K. Birnbaum, Acta Met. 23, 973 (1975).

5. H. K. Birnbaum, Scripta Met. 7, 925 (1973).

6. H. K. Birnbaum and C. A. Wert, Ber. Bunsenges. Phys. Chem. 76, 809 (1972).

7. W. S. Gorsky, Z. Physik S. U. 8, 457 (1935).

8. J. Völkl, Ber. Bunsenges. Phys. Chem. 76, 797 (1972).

9. J. L. Snoek, Physica 8, 711 (1941).

10. J. A. Pryde and C. G. Litcomb, Trans. Faraday Soc. 65, 2758 (1969).

11. W. Gissler, Ber. Bunsenges. Phys. Chem. 76, 770 (1972).

12. C. A. Wert, J. Phys. Chem. Solids 31, 1771 (1970).

13. R. W. Powers and M. V. Doyle, J. Appl. Phys. 30, 514 (1959).

14. R. W. Powers and M. V. Doyle, Trans. AIME 215, 655 (1959).

15. R. Gibala and C. A. Wert, Acta Met. 14, 1095 (1966); R. Gibala and C. A. Wert, Acta Met. 14, 1105 (1966).

16. G. Cannelli and L. Verdini, Ric. Sci. 36, 98 (1966).

17. P. Schiller and A. Scheiders, Int. Conf. on Vacancies and Interstitials in Metals 2, 871 (1968).

18. C. Wert, D. Thompson and O. Buck, J. Phys. Chem. Solids 31, 1793 (1970).

19. G. Schaumann, J. Völkl and G. Alefeld, Phys. Stat. Sol. 42, 401 (1970).

20. P. Schiller and A. Schneiders, Phys. Stat. Sol. (a) 29, 375 (1975).

21. P. Schiller and N. Nijman, Phys. Stat. Sol. (a) 31, K75 (1970).

22. C. P. Flynn and A. M. Stoneham, Phys. Rev. B1, 3966 (1970).

23. H. A. Leupold and H. A. Boorse, Phys. Rev. A134, 1322 (1964).

24. W. R. Heller, Acta Met. 9, 600 (1961).

25. A. M. Stoneham, J. Phys. F: Metal Phys. 6, 167 (1976).

26. J. J. Au and H. K. Birnbaum, Acta Met. 26, 1105 (1977).

27. D. Poker, Ph.D. Thesis, University of Illinois (1979).

28. H. K. Birnbaum and C. P. Flynn, Phys. Rev. Lett. 37, 25 (1976).

29. G. J. Sellers, A. C. Anderson and H. K. Birnbaum, Phys. Rev. B10, 2771 (1974).

30. C. Morkel, H. Wipf and K. Neumaier, Phys. Rev. Lett. 40, 947 (1978).

31. D. G. Westlake, Trans. AIME 245, 287 (1969).

32. A. Seeger, E. Mann and R. v. Jan, J. Phys. Chem. Solids 23, 639 (1962).

33. J. Buchholtz, J. Völkl and G. Alefeld, Phys. Rev. Lett. 30, 318 (1973).

34. H. Metzger, J. Peisl and J. Wanagel, J. Phys. F: Metal Phys. 6, 2195 (1976).

35. G. Bauer and W. Schmatz in Hydrogen Effects on Behavior of Materials, edited by A. W. Thompson and I. M. Bernstein, p. 651, AIME, New York (1975).

36. R. Cantelli, F. M. Mazzolai and M. Nuovo, Phys. Stat. Sol. 34, 597 (1969).

37. G. Matusiewicz, R. Booker, J. Keiser and H. K. Birnbaum, Scripta Met. 8, 1419 (1974).

38. J. Völkl, H. C. Bauer, U. Freudenberg, M. Kokkinidis, G. Lang, K.-A. Steinhauser and G. Alefeld, Proc. of the Int. Conf. on Internal Friction and Ultrasonic Attenuation in Solids, p. 485, Tokyo (1977).

39. H. Wipf and G. Alefeld, Phys. Stat. Sol. (a) 23, 175 (1974).

40. W. Münzing, J. Völkl, H. Wipf and G. Alefeld, Scripta Met. 8, 1327 (1974).

41. D. Richter, J. Töpler and T. Springer, J. Phys. F: Metal Phys. 6, L93 (1976).

42. G. Pfeiffer and H. Wipf, J. Phys. F: Metal Phys. 6, 167 (1976).

43. R. Hanada, Second International Congress on Hydrogen in Metals, 1B6, Paris (1977).

44. A. S. Nowick and B. S. Berry, Anelastic Relaxation in Crystalline Solids, Academic Press, New York (1972).

45. A. S. Nowick and W. R. Heller, Adv. Phys. 12, 251 (1963).

46. A. S. Nowick and W. R. Heller, Adv. Phys. 14, 101 (1965).

47. A. S. Nowick, J. Phys. Chem. Solids 34, 1507 (1973).

48. A. S. Nowick, Adv. Phys. 16, 1 (1967).

49. C. Wert and C. Zener, Phys. Rev. 76, 1169 (1949).

50. J. A. Sussmann, Ann. Phys. (Paris) 6, 135 (1971).

51. A. M. Stoneham, Coll. Phen. 2, 9 (1975).

52. A. M. Stoneham, J. Nuc. Mat. 69 & 70, 109 (1978).

53. A. M. Stoneham, J. Phys. F: Metal Phys. 2, 417 (1972).

54. R. Truell, C. Elbaum and B. Chick, Ultrasonic Methods in Solid State Physics, Academic Press, New York (1969).

55. T. G. Digges, Jr. and M. Achter, Trans. AIME 230, 1739 (1964).

56. E. Fromm and H. Jehn, Met. Trans. 3, 1685 (1972).

57. E. Velekis, Ph.D. Thesis, Illinois Institute of Technology (1960).

58. E. Fromm and H. Jehn, Vacuum 19, 191 (1969).

59. J. P. Hirth and J. Lothe, Theory of Dislocations, McGraw Hill, New York (1968).

60. P. Matyash, N. Skakun and N. Dikii, JETP Letters 19, 18 (1974).

61. H. D. Carstanjen, Ion Beam Surface Layer Analysis, edited by O. Mayer, G. Lisker and F. Käppler, p. 497, Plenum Press, New York (1976).

62. J. C. Fisher, Acta Met. 6, 13 (1958).

63. R. A. Johnson, G. J. Dienes and A. C. Damask, Acta Met. 12, 1215 (1964).

64. M. S. Blanter and A. G. Khachaturyan, Met. Trans. 9A, 753 (1978).

65. H. Pfeiffer and H. Peisl, Phys. Lett. 60A, 363 (1977).

66. D. A. Reed and G. Ehrlich, J. Chem. Phys. 64, 4616 (1976).

67. J. Buchholtz, International Conference on Hydrogen in Metals, p.544, Jülich (1972).

68. C. Heiple, Ph.D. Thesis, University of Illinois (1967).

69. P. Bevington, Data Reduction and Error Analysis for the Physical Sciences, p. 232, McGraw-Hill, New York (1969).

70. A. Taylor and N. J. Doyle, J. Less-common Met. 13, 313 (1967); A. Taylor and N. J. Doyle, J. Less-common Met. 13, 399 (1967).

71. E. Gebhart and R. Rothenbacher, Z. Metallk. 54, 443 (1963).

72. E. Gebhart, W. Durchschnabell and G. Hörz, J. Nucl. Mat. 18, 119 (1966).

73. D. Park, Introduction to Quantum Theory, McGraw-Hill, New York (1964).

VITA

Philip Emerson Zapp was born on [redacted] After graduation from high school in Millburn, New Jersey, he attended Cornell University, where he received the Bachelor of Arts degree in Physics in 1971. From 1971 to 1978 he held a graduate research assistantship in the Department of Metallurgy and Mining Engineering and the Materials Research Laboratory of the University of Illinois at Urbana-Champaign.

ANELASTIC STUDIES OF INTERSTITIALLY TRAPPED HYDROGEN IN NIOBIUM

Philip Emerson Zapp, Ph.D.
Department of Metallurgy and Mining Engineering
University of Illinois at Urbana-Champaign, 1979

An experimental study of the local motion of hydrogen trapped by oxygen and nitrogen solutes has been conducted using anelastic relaxation methods. Internal friction peaks due to the reorientation of O-H pairs were measured with a pulse-echo ultrasonic attenuation technique in the ⟨100⟩, ⟨110⟩, and ⟨111⟩ directions of niobium single crystals. Reorientation occurs by hydrogen jumping around the fixed O interstitial trap, the frequency of which was found to be higher in the ⟨111⟩ direction than in the ⟨100⟩ direction. The activation enthalpy of motion was 0.12 eV in the former direction and 0.18 eV in the latter. Two probable models for the O-H defect are (1) a single O-H pair with ⟨100⟩ monoclinic point symmetry, and (2) two types of pairs, one with ⟨100⟩ orthorhombic symmetry and the other with ⟨110⟩ monoclinic symmetry.

The jump frequency of nitrogen-trapped hydrogen in the temperature range of about 40 to 80K was studied with strain relaxation and low frequency internal friction techniques. The jump frequency at a given temperature was found to be lower than that of oxygen-trapped hydrogen, and it is in good agreement with the Flynn-Stoneham theory of phonon-assisted quantum tunnelling.